様式 2-4-1

日米科学技術協力事業「脳研究」分野
グループ共同研究実施報告書　〔研究分野：　2　〕

1．グループ共同研究代表者
京都大学医学研究科・教授・河野憲二

2．研究課題名
視覚的眼球運動制御の神経機構

3．日本側グループ組織（代表者及び分担者の所属・職・氏名）
代表者：京都大学大学院医学研究科・教授・河野憲二
分担者：京都大学大学院医学研究科・科学技術振興助手・三浦健一郎
分担者：京都大学大学院・大学院生（博士課程）・松浦清人

4．米国側グループ組織（代表者及び分担者の所属・職・氏名）
代表者：National Eye Institute, NIH・Sect. Chief・F.A. Miles
分担者：National Eye Institute, NIH・Act.. Chief・L.M. Optican

5．研究期間　平成１６年　４月　１日～平成１９年　３月３１日

6．研究の概要，成果及び意義
広視野の視覚刺激が動く時、脳は時々刻々変化する網膜像からその動きを検出し、追従眼球運動と呼ばれる合目的的な眼球運動を起こすことによって網膜像の「ぶれ」を抑える。脳がこの視覚性眼球運動を発現する時の情報処理を明らかにすることを目的として研究を進めてきた。これまでに共同で行ってきた実験的研究の結果から、霊長類が視覚的眼球運動を生成する時に行う、動視覚刺激の解析のメカニズムについて新たな事実がわかった。平成１６年度に脳が追従眼球運動を起こす時の網膜像の動きの解析メカニズムの詳細を調べるための共同研究をNIHの当該グループと開始した。脳が行う動き検出には輝度の時空間的変化から視覚刺激の動きを検出する一次運動検出メカニズムとさらに高次な特徴から動きを検出するメカニズムがあるが、追従眼球運動にそのどちらが関係するかを調べることのできる実験課題を米国側研究者と共に作成してサルの追従眼球運動を調べた。その結果、サルの追従眼球運動を発生する時の視覚刺激の動きを解析するメカニズムが、一次運動検出メカニズムであることを強く示唆する所見を得た。さらに、互いに動きの方向が異なる二つの縞を合成した重畳視覚刺激、互いに動きの速度が異なる二つの縞を合成した重畳視覚刺激を用いて、その視覚刺激の処理間の相互作用を調べるための実験課題を米国側の研究者と共に作成し、サルの追従眼球運動を調べた。その結果、重畳視覚刺激の動きで起こった追従眼球運動が、重畳視覚刺激に含まれるそれぞれの要素刺激単独の動きで起こる追従眼球運動の重み付け平均によって再構成できることがわかった。この追従眼球運動の特性は、運動指令を構築する過程の中に、初期の動き検出器によって検出された信号間に競合的なメカニズムを仮定する運動指令構築モデルで良く説明できる。また、米国側では同じ視覚刺激を用いてヒトの眼球運動を調べていたが、サルのこの運動検出機構がヒトの追従眼球運動発生の基盤となるものと、非常に似ていることが示された。これらの研究成果は、サルがヒトの追従眼球運動発生の基盤的メカニズムを詳しく調べる時の良いモデルとなることを示すと共に、追従眼球運動制御の運動指令構築過程を理解するための重要な情報を提供すると考えている。

7．その他（実施上の問題点，特記事項等）

サルが追従眼球運動を起こす時の網膜像の動きの解析メカニズムの詳細を調べるために行った実験の結果の一部は、共同研究の成果として２００５年の Annual meeting of Society for Neuroscience(WashingtonDC で開催)で成果発表を行った。この研究の詳細をまとめた論文（米国側共同研究者との共著）は平成１７年度（２００６年）に Vision Research に掲載された（別刷を参考資料として添付)。さらに、上記の、互いに動きの方向が異なる二つの縞を合成した重畳視覚刺激、互いに動きの速度が異なる二つの縞を合成した重畳視覚刺激を用いて行った、視覚刺激の処理間の相互作用を調べる研究の結果の一部は２００６年に京都で行われた日本神経科学学会において共同研究の成果として発表し、現在、米国側と共著論文原稿の作成を行っている。これらは Vision Research への投稿を予定している。また、サルを用いた破壊実験で追従眼球運動の発現に大脳 MT,MST 野が関与していることを明らかにした論文（米国側共同研究者との共著、別刷を参考資料として添付）を Journal of Neuroscience 誌に発表した。

◎参考資料があれば，添付ください。

Behavioral/Systems/Cognitive

# Deficits in Short-Latency Tracking Eye Movements after Chemical Lesions in Monkey Cortical Areas MT and MST

**Aya Takemura,[1] Yumi Murata,[1,2] Kenji Kawano,[1,3] and F. A. Miles[4]**

[1]Neuroscience Research Institute, National Institute of Advanced Industrial Science and Technology, Tsukuba, Ibaraki 305-8568, Japan, [2]Graduate School of Comprehensive Human Science, University of Tsukuba, Tsukuba, Ibaraki 305-8574, Japan, [3]Department of Integrative Brain Science, Graduate School of Medicine, Kyoto University, Kyoto 606-8501, Japan, and [4]Laboratory of Sensorimotor Research, National Eye Institute, National Institutes of Health, Bethesda, Maryland 20892

**Past work has suggested that the medial superior temporal area (MST) is involved in the initiation of three kinds of eye movements at short latency by large-field visual stimuli. These eye movements consist of (1) version elicited by linear motion (the ocular following response), (2) vergence elicited by binocular parallax (the disparity vergence response), and (3) vergence elicited by global motion toward or away from the fovea (the radial-flow vergence response). We investigated this hypothesis by recording the effects of ibotenic acid injections in the superior temporal sulcus (STS) of both hemispheres in five monkeys. After the injections, all three kinds of eye movements were significantly impaired, with the magnitude of the impairments often showing a strong correlation with the extent of the morphological damage in the three subregions of the STS: dorsal MST on the anterior bank, lateral MST and middle temporal area on the posterior bank. However, the extent of the lesions in the three subregions often covaried, rendering it difficult to assess their relative contributions to the various deficits. The effects of the lesions on other aspects of oculomotor behavior that are known to be important for the normal functioning of the three tracking mechanisms (e.g., ocular stability, fixation disparity) were judged to be generally minor and to contribute little to the impairments. We conclude that, insofar as MST sustained significant damage in all injected hemispheres, our findings are consistent with the hypothesis that MST is a primary site for initiating all three visual tracking eye movements at ultra-short latencies.**

*Key words:* **visual tracking eye movement; ocular following response; vergence; disparity; optic flow; radial flow; extrastriate; ibotenic acid; oculomotor; visual motion**

## Introduction

Recent studies in primates have revealed three visually driven ocular tracking mechanisms that are activated in a machine-like manner at ultra-short latencies and are thought to help to stabilize the gaze of the moving observer in three dimensions (Miles, 1998). In this scheme, two of these mechanisms generate vergence eye movements to help maintain binocular alignment on objects that lie ahead: the disparity vergence response (DVR), which is driven by the changes in binocular parallax (Busettini et al., 1996; Masson et al., 1997), and the radial-flow vergence response (RFVR), which is driven by the radial patterns of optic flow (Busettini et al., 1997; Inoue et al., 1998b). The third mechanism, the ocular following response (OFR), helps to stabilize gaze on objects that move within the plane of fixation and generates version eye movements in response to the planar motion (Kawano and Miles, 1986; Miles and Kawano, 1986; Miles et al., 1986).

This study is concerned with the neural mediation of these responses and focuses on the role of the medial superior temporal area (MST) within the superior temporal sulcus (STS) of the monkey's cortex. This area is known to contain many neurons that respond vigorously to visual motion with directional selectivity (Van Essen et al., 1981; Desimone and Ungerleider, 1986) and others that are sensitive to binocular disparity or to the patterns of optic flow experienced by the moving observer (Maunsell and Van Essen, 1983a; Tanaka et al., 1986; Tanaka and Saito, 1989; Roy and Wurtz, 1990; Duffy and Wurtz, 1991; Roy et al., 1992; Eifuku and Wurtz, 1999). We have recorded neurons in MST that discharge in relation to the large-field visual stimuli used to elicit the OFR (Kawano et al., 1994; Takemura et al., 2000), the DVR (Takemura et al., 2001, 2002b) and the RFVR (our unpublished observations). Most of the changes in neural activity preceded the associated eye movements, and some occurred early enough for them to have a causal role in producing even the earliest ocular responses. These electrophysiological experiments suggested that, despite their ultra-short latency, all three visual tracking eye movements could be mediated, at least in part, by MST neurons.

Received Aug. 10, 2006; revised Dec. 8, 2006; accepted Dec. 10, 2006.

This work was supported by the Special Coordination Funds for Promoting Science and Technology, the Japan Science and Technology Agency–Exploratory Research for Advanced Technology Shimojo project, Japan Society for the Promotion of Science–KAKENHI (16GS0312), and Ministry of Education, Culture, Sports, Science and Technology–KAKENHI (17022019). We thank Y. Inoue for support during the early phase of this work. We are grateful to M. Okui, A. Muramatsu, and T. Takasu for skillful technical assistance and K. Nagatsuka for secretarial help.

Correspondence should be addressed to Dr. Aya Takemura, Neuroscience Research Institute, National Institute of Advanced Industrial Science and Technology, 1-1-1, Umezono, Tsukuba, Ibaraki 305-8568, Japan. E-mail: a.takemura@aist.go.jp.

DOI:10.1523/JNEUROSCI.3455-06.2007

 0270-6474/07/270529-13$15.00/0

The present study was undertaken to test this hypothesis by documenting the effects of bilateral chemical lesions in the STS, which included varying amounts of dorsal MST (MSTd), lateral MST (MSTl), and middle temporal area (MT), on the three short-latency visual tracking eye movements in five monkeys. We report that ibotenic acid injections into the STS could abolish the initial OFR and the initial RFVR and significantly attenuate the initial DVR. These findings are consistent with our hypothesis that the MST has a major role in the production of all three of these ocular tracking responses.

Preliminary results have been reported previously (Takemura et al., 2002a).

## Materials and Methods

*Animal preparation.* Data were collected from five adolescent Japanese monkeys (*Macaca fuscata*), weighing 5–9 kg. Many of the methods and procedures were very similar to those used in our previous studies (Kawano et al., 1994; Inoue et al., 1998b; Takemura et al., 2001) and will be described only briefly here. All animals had been trained previously to fixate a small target spot on a tangent screen for a liquid reward (Wurtz, 1969). Under aseptic conditions and sodium pentobarbital anesthesia, a cylinder for chronic recording of single neuron activity was implanted vertically over a trephine hole positioned above the posterior parietal cortex. This cylinder was subsequently used for the ibotenic acid injections. A bracket attached to the skull allowed the head to be secured in the standard stereotaxic position during the experiments. Eye movements were recorded using scleral search coils implanted around both eyes (Fuchs and Robinson, 1966; Judge et al., 1980). One animal (monkey P) had been used previously for single-unit recordings in the left nucleus of the optic tract (NOT) and in the left dorsolateral pontine nucleus (DLPN), but its oculomotor behavior was within the normal limits after those recordings. All experimental protocols were approved by the National Institute of Advanced Industrial Science and Technology Animal Care and Use Committee.

*Behavioral paradigms and visual stimuli.* The presentation of stimuli and the collection, storage, and display of data were controlled by two personal computers (NEC PC98). The behavioral paradigms and visual stimuli used in this study were identical to those of Shidara and Kawano (1993) for the OFR, Takemura et al. (2001) for the DVR, and Inoue et al. (1998b) for the RFVR. In brief, during the recording sessions, the monkey sat in a primate chair with its head secured in place and facing a translucent tangent screen (114 × 114 cm) at a distance of 500 mm onto which random-dot patterns (subtense, 90 × 90°) could be backprojected. Mirror galvanometers in the projection path in an *X*/*Y* configuration allowed the patterns to be moved under computer control. The density of dots was ~50%, and the smallest dots in the patterns subtended ~1.5° of arc. Five paradigms were used, which in brief were as follows.

In the OFR paradigm, the random-dot pattern filled the screen and 50 ms after the end of a 10° leftward centering saccade started to move at constant velocity (range, 10–160°/s) in one of the four cardinal directions; the motion lasted 150 ms, and the screen was blanked. In the DVR paradigm, two projectors were used with crossed polarizers to achieve dichoptic viewing such that the two eyes saw identical random-dot patterns that filled the screen and initially overlapped exactly (zero binocular disparity); horizontal disparity steps (crossed and uncrossed, ranging in amplitude from 0.5 to 6°) were applied 50 ms after 10° leftward centering saccades, by displacing the two images equally in opposite directions for 230 ms. In the RFVR paradigm, the visual stimulus was a two-frame movie, and the initial random-dot pattern was replaced by a second one (simulating the same image viewed from a slightly different distance) 50 ms after a leftward centering saccade. The focus of expansion/contraction was located at the center of the screen and was therefore imaged in, or close to, the fovea; this looming step involved a 5% change in the eccentricity of the dots with respect to the screen center without any change in their size [the "pure radial-flow stimulus" (Busettini et al. (1997)]. Note that previous studies indicated that the RFVR is mostly a transient response to stimulus onset and multiple steps (at up to 100 Hz, which approximates smooth motion) elicit essentially the same result (i.e., adding additional apparent-motion steps adds little to the response) (Miles et al., 2004). In all three paradigms, if no saccades were detected during the stimulus presentation period, then the data were stored on a hard disk and the animal was given a drop of fruit juice; otherwise, the trial was aborted and fluid was withheld. At this point, the random-dot patterns were blanked for 0.5 s by a mechanical shutter and then reappeared once more for the start of the next trial. Note that all experiments included saccade-only controls in which the initial patterns remained present and unchanging throughout the trial. The luminance of the patterns ranged from 2.7 cd/m$^2$ (white dots) to 0.3 cd/m$^2$ (black background area) for the RFVR paradigm (average, 1.5 cd/m$^2$) and from 1.0 to 0.05 cd/m$^2$ for the DVR paradigm (average, 0.5 cd/m$^2$). The stimulus patterns used for the DVR paradigm were somewhat darker than those used for RFVR paradigm because of the polarizing filters. The brighter stimulus pattern was also used for the OFR paradigm, except with monkeys N and R for which the polarizers remained in place (but the dichoptic images always exactly overlapped).

In two monkeys, we also examined the effects of the MST injections on smooth-pursuit and optokinetic eye movements to permit comparison with previous lesion studies (Dürsteler et al., 1987; Dürsteler and Wurtz, 1988). In the smooth-pursuit paradigm, the target was a projected light-emitting diode spot, the horizontal position of which was controlled by a mirror galvanometer in the projector light path. At the start of each trial, a stationary target spot appeared at the center of the screen, and the monkey was required to fixate it for 700–900 ms. On "pursuit" trials, the target moved to the right or left at one of three selected speeds (10, 20, 30°/s), and after a grace period of 100 ms to allow the monkey to catch up with the target, the monkey was required to track it with smooth eye movements for the remaining time that it was visible (600 ms). On "fixation" trials, the target remained stationary, and the monkey had to fixate it. The trial type (pursuit or fixation) as well as the direction and speed of target motion on the pursuit trials were randomized from trial to trial. In the optokinetic paradigm, two random-dot patterns moving to the right or left at one of three selected speeds (20, 40, 60°/s) were backprojected on the screen one after the other to achieve continuous smooth motion. To replicate the traditional optokinetic stimulation used in previous lesion studies, the screen was initially dark, and then the moving pattern suddenly came into view (by operating a shutter). This optokinetic stimulus remained on for 15 s, after which time the screen was blanked and recording continued for an additional 15 s [optokinetic afternystagmus (OKAN)]. The monkey was rewarded with drops of fluid for staying alert (apparent from the brisk quick phases).

*Lesion procedures.* Previous microelectrode recordings, involving 10–64 penetrations per hemisphere, allowed us to determine the likely location of the MST within the STS of both hemispheres in all five monkeys. In 7 of 10 hemispheres, the penetrations were made with glass-coated tungsten microelectrodes that entered the parietal cortex, advanced through the anterior bank of the STS, and ended in the posterior bank or floor of the STS. After reconstructing these penetrations and using the selectivity for speed and direction of motion as well as the size of the receptive fields to identify putative MT and MST neurons in both hemispheres, we implanted four or five guide tubes, the tips of which were positioned 3–5 mm above the regions thought to encompass the MST in both hemispheres. These guide tubes were to be used later for injecting ibotenic acid, but we first used them to introduce tungsten microelectrodes to confirm that they were located above a region containing abundant directionally selective neuronal activity characteristic of MT and MST. In 3 of 10 hemispheres, the neuronal recordings were made only through the guide tubes, and accurate reconstruction of these electrode tracks was not possible.

The preinjection eye-movement data were obtained over a period of several days after the guide tubes had been positioned in both hemispheres. Thus, any effects attributable to the previous microelectrode penetrations and the implantation of the guide tubes would be manifest in the eye-movement data obtained before any injections were made. After completing the collection of the preinjection data, these guide tubes were used to make multiple pressure injections of ibotenic acid (15 mg/ml in a basic saline solution) over a 2 d period in monkeys Q, P, and S; a 3 d period in monkey N; and a 7 d period in monkey R. We used a

**Table 1. Number and volume of the ibotenic acid injections**

| | Left STS | | | Right STS | | | |
|---|---|---|---|---|---|---|---|
| | Number of guide tubes | Number of injection sites (volume, μl) | | Number of guide tubes | Number of injection sites (volume, μl) | | Total volume (μl) |
| | | Anterior bank | Posterior bank | | Anterior bank | Posterior bank | |
| Monkey Q | 4 | 4 (8.0) | 4 (8.0) | 4 | 4 (8.0) | 4 (8.0) | 32.0 |
| Monkey N | 5 | 6 (12.3) | 5 (10.1) | 4 | 4 (8.0) | 3 (6.0) | 36.4 |
| Monkey P | 4 | 5 (9.4) | 4 (8.0) | 5 | 5 (10.0) | 5 (10.0) | 37.4 |
| Monkey R | 5 | 6 (24.0) | 5 (22.7) | 5 | 5 (10.0) | 5 (10.0) | 66.7 |
| Monkey S | 4 | 5 (10.0) | 4 (8.1) | 4 | 5 (10.0) | 4 (8.0) | 36.1 |

Hamilton microsyringe (Crist Instruments, Hagerstown, MD) with a 0.7 mm outer-diameter injection tube, to inject at a rate of 0.2 μl/min, which subsequent histology indicated was sufficiently slow to prevent backflow of ibotenic acid around the microsyringe. To avoid leakage of ibotenic acid during withdrawal, the microsyringe was not raised for at least 15 min after completion of the injection(s) through a given guide tube. The number of injection sites and total amount of ibotenic acid injected are summarized in Table 1. For each monkey, the postinjection eye-movement data were obtained over a period of 2–3 d commencing 1 d after completing the bilateral injections.

*Data collection and assessment of the eye-movement deficits.* In the OFR paradigm, we recorded only the horizontal and vertical positions of the right eye. In the DVR and RFVR paradigms, we recorded only the horizontal positions of both eyes. The eye-position measures were hardware differentiated to obtain eye velocity measures. These position and velocity voltage signals were smoothed with a six-pole Bessel filter (3 dB at 100 Hz) and digitized at 1000 Hz with a resolution of 12 bits. Voltage signals encoding the positions of the mirror galvanometers controlling the positions of the patterns and target spots on the screen were digitized at 500 Hz with a resolution of 12 bits. All data were stored and transferred to a workstation (SunSparc) for analysis. Trials with saccadic intrusions during the experiment were deleted. The mean eye velocity data obtained in the saccade-only control trials were subtracted from the eye velocity data obtained in all other trials, and all quantitative analyses were performed on these "adjusted" data profiles. The horizontal eye position and velocity data obtained in the DVR and RFVR paradigms were used to compute the horizontal vergence position angle and the horizontal vergence velocity (left eye minus right eye), respectively. We used the convention that rightward (and upward) deflections of the stimuli or eyes were positive; hence convergence had a positive sign. Mean response profiles to a particular stimulus over time, synchronized to stimulus onset (time 0), were computed for eye position, eye velocity, horizontal vergence position, and vergence velocity for the complete data sets obtained before and after the injections. Mean eye acceleration profiles were obtained by digital differentiation of the mean eye velocity data and were used to estimate the latency of onset of the OFR (criterion for onset, $100°/s^2$). The initial open-loop OFRs were quantified by measuring the change in the position of the right eye over the time period 50–100 ms measured from stimulus onset. The initial open-loop DVRs and RFVRs were quantified by measuring the change in vergence position over the same time period. To assess the magnitude of the deficits in the ocular responses after the ibotenic acid injections, we calculated a percentage reduction, defined as $[(R_{pre} - R_{post})/R_{pre}] \times 100\%$, where $R_{pre}$ and $R_{post}$ are the response measures for the initial open-loop OFR, DVR, or RFVR before and after the injections, respectively.

*Morphological reconstruction of the locations and extents of the lesions.* At the conclusion of the postinjection recordings from a given monkey, that animal was deeply anesthetized with sodium pentobarbital and perfused through the heart with normal saline followed by 10% formalin. The animal's brain was removed, and 50 μm frozen sections were cut in the sagittal plane. After mounting on microscope slides, sections were stained with cresyl violet for cell bodies and with a modified silver stain for myelinated fibers (Gallyas, 1979). Maps of the STS region of the cortex were created, based on the method of Van Essen and Maunsell (1980), and the extent of the lesions was drawn on these maps (see Fig. 1). The densely myelinated zones (DMZs) in the posterior bank (MT) and in the anterior bank (DMZ) were identified and transferred onto the unfolded maps (Newsome et al., 1985; Ungerleider and Desimone, 1986). Because the former zone corresponds to the MT area, the latter zone will be referred to as the DMZ (densely myelinated zone) from here on. In locating MST, we followed the precedent of Komatsu and Wurtz (1988), who defined it as that region of the STS outside MT that contains a preponderance of directionally selective neurons. These workers showed that neurons in MST could be distinguished from neurons in MT by their larger field size for a given retinal eccentricity and that the rostrocaudal extent of MST was definable morphologically, encompassing the DMZ anteriorly and extending up to the boundary of MT posteriorly, but the mediolateral boundaries had no exact morphological correlates. In estimating the extent of the involvement of MST in our lesions, we have assumed that the MST encompassed the entire region of the STS extending between the two myelinated zones, with MSTl occupying the posterior bank and MSTd occupying the anterior bank (Komatsu and Wurtz, 1988). The areas affected by the ibotenic acid injections were identified using the morphological criteria of Newsome et al. (1985). Surface area measurements of the lesions and the various subdivisions of the STS were made from the maps with the use of a scanner and a program designed for measuring area.

## Results

### Reconstruction of the STS lesions

Maps of the STS region of the cortex, reconstructed from sagittal sections, are shown in Figure 1 for all 10 hemispheres that were injected in five monkeys. To facilitate easy comparisons of the lesions on the two sides of the brain, maps from the left hemisphere are left–right reversed. The densely myelinated zones in the posterior bank (MT) and in the anterior bank (DMZ) were identified together with the locations of 23 neurons recorded in 8 penetrations that were deemed to be MT neurons (Fig. 1, filled red circles) and an additional 127 neurons that were recorded in 21 penetrations and deemed to be MST neurons (Fig. 1, filled green circles). These recordings were made with rigid glass-coated microelectrodes advanced through the depth of the cortex, permitting reconstruction of the entire penetration from the surface of the cortex to the floor of the STS. (All neuronal recordings in both hemispheres of monkey R and in the left hemisphere of monkey Q were done with flexible microelectrodes introduced through the guide tubes subsequently used for the ibotenic acid injections. An accurate reconstruction of these electrode tracks was not attempted.) Although these electrophysiological recordings provided good confirmation of the locations of some parts of MST, and proved useful for positioning the guide tubes over the putative MST region, it is evident from Figure 1 that they were generally not sufficient to define the exact mediolateral extent of the MST. In specifying its mediolateral boundaries in Figure 1, we assumed that MST encompassed the entire region of the STS between the MT and the DMZ with a slight medial extension (Fig. 1, dashed lines). We will use the floor of the sulcus of the STS to subdivide the MST into an anterior region that approximates MSTd and a posterior region that approximates MSTl. Table 1 summarizes the number of guide tubes and injection sites together with the volume of ibotenic acid injected in each monkey. The initial injections in monkey R were ineffective (probably because the ibotenic acid was not fully dissolved), and a second series was required, hence the unusually large volume in that monkey. The regions affected by the ibotenic acid injections were

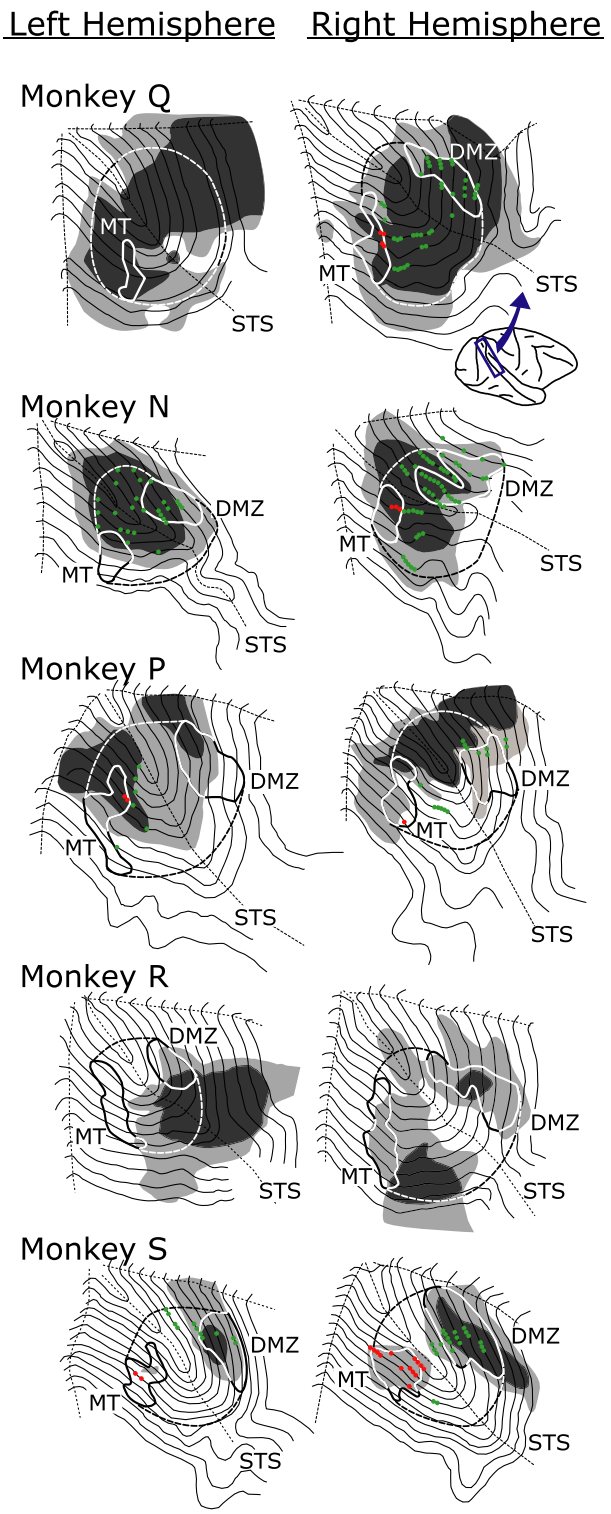


**Figure 1.** Two-dimensional maps of the STS in 10 hemispheres of five monkeys reconstructed from parasagittal sections using the method of Van Essen and Maunsell (1980). The maps of the left hemisphere are left–right reversed to facilitate easy comparison with the maps of the right hemisphere. The inset shows a view of the right hemisphere with the general area of the STS indicated. Contour lines depict the unfolded layer IV. Solid boundary lines delineate the densely myelinated zones in the anterior bank (DMZ) and the posterior bank (MT) of the STS. Dashed lines depict the approximate medial and lateral boundaries of the MST, which is subdivided into MSTd anteriorly and MSTl posteriorly by the dotted lines depicting the floor of the STS. Black shading indicates areas with morphological damage extending through all layers of the cortex (complete lesion), and gray shading indicates areas with damage to some but not all cortical layers (partial lesions). Circles indicate the approximate recording sites of neurons that responded to visual motion and showed directional selectivity (red, MT neurons; green, MST neurons).

identified using the morphological criteria of Newsome et al. (1985) and were subdivided into areas in which all six layers were affected (designated as "complete" lesions) (Fig. 1, black) and into areas in which only some layers showed morphological changes (designated as "partial" lesions) (Fig. 1, gray). The background silver stain in the lesioned areas sometimes obscured the dense myelination, leading us to underestimate the full extent of MT and the DMZ in those cases. This was especially true on the left side in monkey Q, where we were unable to discern the DMZ (and so assumed that it had been completely lesioned); in this case, the boundary of MST was drawn to approximate that on the opposite side.

Table 2 has three sections that each summarizes our quantitative estimates of the extent of the partial and/or complete lesions in one of the three subregions of the STS (MSTd, MSTl, MT) in both hemispheres for each of the five monkeys. The entries in each section indicate the area in square millimeter of the morphological changes within the given subregion; in addition, these values are each expressed as a percentage of the area of their respective subregion (entries in parentheses), and we will refer to these as the "percentage of extent" of the lesions. Note that the "total" area of the lesions refers to their overall extent and is given by the sum, "partial plus complete." The extent of the lesions varied considerably among the five monkeys, and the order in which their data are shown in Figure 1 and listed in Table 2 (Q, N, P, R, S) generally accords with their percentage total lesions, which were largest in monkey Q and smallest in monkey S. In monkey Q, these total lesions included much of MST and MT on both sides. However, in monkeys N and P, significant portions of MST on both sides (especially laterally) as well as the lateral (foveal) regions of MT on the left side were completely spared, and in monkeys R and S, even more of MST (especially the floor of the sulcus and the posterior bank in monkey S bilaterally) and almost all of MT on the left side were intact. Bilateral asymmetries, based on the differences in the percentage of total lesions in the two hemispheres of a given monkey, were generally minor for MST, averaging only 9% for MSTd (range, 0–15%) and 15% for MSTl (range, 1–35%), but could be appreciable for MT, averaging 41% (range, 0–90%). The proportions of the three subdivisions of the STS that sustained damage to all layers (complete lesion) ranged from 0 to 100% and were <50% in two-thirds (20 of 30) of the cases listed in Table 2. It is perhaps not surprising that the percentage extents of the lesions in a given subdivision of a given monkey tended to be positively correlated and the $r^2$ values for the complete lesion data were very high: 0.97 for MSTl versus MSTd, 0.93 for MST versus MT, 0.85 for MSTl versus MT, and 0.95 for MSTd versus MT. The equivalent $r^2$ values for the total lesion data were much lower: 0.71, 0.49, 0.28, and 0.77. Note that there was clear gliosis along the path of the guide tubes in the overlying area 7a but there was no evidence of any additional damage such as might be expected from ibotenic acid because of backflow around the microsyringe or leakage during withdrawal of the microsyringe.

### OFRs

The initial OFRs recorded before the injections of ibotenic acid were like those described by Miles et al. (1986) in all essentials, with onset latencies of 55–60 ms and mean eye velocity temporal profiles that showed an initial brisk increase, followed by a slight hesitation and perhaps a second transient increase, before giving way to a more gradual and sustained buildup (Fig. 2, thick traces). After the injections, the mean eye velocity temporal profiles showed varying degrees of attenuation (Fig. 2, thin traces). Onset

**Table 2. Estimated area of the lesions in the three subregions of the STS**

| | Left MSTd | | | Right MSTd | | |
|---|---|---|---|---|---|---|
| | Partial | Complete | Total | Partial | Complete | Total |
| Monkey Q | 55.2 (17) | 208 (65) | 263.2 (83) | 37 (19) | 157.2 (79) | 194.1 (98) |
| Monkey N | 55.5 (30) | 122.1 (67) | 177.6 (97) | 70 (35) | 99.5 (50) | 169.5 (85) |
| Monkey P | 182.8 (58) | 31.7 (10) | 214.5 (69) | 75.2 (32) | 88.1 (37) | 163.3 (69) |
| Monkey R | 27.1 (22) | 44.7 (37) | 71.9 (59) | 133.8 (55) | 25.6 (10) | 159.4 (65) |
| Monkey S | 72.5 (34) | 26.9 (12) | 99.4 (46) | 85.3 (31) | 77 (28) | 162.4 (58) |
| | Left MSTl | | | Right MSTl | | |
| | Partial | Complete | Total | Partial | Complete | Total |
| Monkey Q | 83.7 (36) | 148.8 (63) | 232.4 (99) | 53.5 (19) | 228.3 (81) | 281.8 (100) |
| Monkey N | 47.1 (31) | 90.4 (60) | 137.6 (91) | 78.2 (39) | 80 (40) | 158.1 (79) |
| Monkey P | 96.3 (36) | 92.6 (35) | 188.9 (70) | 15.7 (9) | 47.2 (26) | 62.8 (35) |
| Monkey R | 55.6 (39) | 43 (30) | 98.6 (69) | 135.4 (47) | 83.9 (29) | 219.2 (76) |
| Monkey S | 0 (0) | 0 (0) | 0 (0) | 20.9 (18) | 0 (0) | 20.9 (18) |
| | Left MT | | | Right MT | | |
| | Partial | Complete | Total | Partial | Complete | Total |
| Monkey Q | 0 (0) | 26.9 (100) | 26.9 (100) | 26 (50) | 26.4 (50) | 52.4 (100) |
| Monkey N | 13.6 (36) | 9.9 (26) | 23.4 (63) | 20.8 (49) | 21.4 (51) | 42.2 (100) |
| Monkey P | 21.8 (28) | 25.9 (33) | 47.7 (60) | 29.0 (51) | 8.9 (16) | 37.9 (67) |
| Monkey R | 3.2 (5) | 0 (0) | 3.2 (5) | 52.8 (74) | 2.6 (4) | 55.4 (78) |
| Monkey S | 3.3 (7) | 0 (0) | 3.3 (7) | 54.6 (97) | 0 (0) | 54.6 (97) |

Values are areas in square millimeter. The proportions of the three subregions affected by the lesions are given in parentheses (percentage). Partial, Areas that have sustained damage to some but not all layers of the cortex; Complete, areas that have sustained damage to all layers of the cortex; Total, areas that have sustained any damage to any layer of the cortex (partial plus complete).

latencies before and after the injections were not significantly different in the three monkeys (N, R, S), whose postinjection responses were large enough to permit measurements of latency (Student's $t$ test, $p > 0.05$).

The quantitative effects of the injections on the initial (open-loop) OFRs, based on the change in eye position over the time period 50–100 ms (measured from stimulus onset), are summarized in Figure 3. For each of the five monkeys and the four cardinal directions of stimulus motion, Figure 3 shows histograms indicating the mean percentage reductions in the OFR measures (averaged across the five different speeds). These measures indicated that all monkeys exhibited significant impairments in their initial OFRs after the injections (Student's $t$ test, $p < 0.05$), the mean percentage reductions for a given direction of motion ranging from 37 to 97%. There were some directional asymmetries in the deficits, and we quantified them by computing the right–left, up–down, horizontal–vertical differences; these data are also shown in Figure 3. The largest consistent directional asymmetries involved relative sparing of the rightward responses in monkeys N, S, and P, and the deficits to leftward motion exceeded those to rightward motion, on average, by 28, 18, and 11%, respectively. The vertical deficits were larger than the horizontal in monkeys Q, N, P, and S, on average, by 6–21%; the fifth monkey, R, showed the reverse asymmetry, with the horizontal deficits exceeding the vertical, on average, by 30%. The graph in Figure 4 plots the percentage of reductions in the OFR measures (averaged across all four cardinal directions) against speed for each of the five monkeys and indicates a tendency for the deficits to be somewhat greater for the data obtained with stimuli moving at the higher speeds.

Scrutiny of Table 2 and Figure 3 suggested that there was a general tendency for the animals with the larger lesions to show larger deficits in their OFRs. We examine this further in Figure 5, in which the mean percentage reductions in the OFR measures (averaged across all stimulus speeds and directions) for each of the five monkeys are plotted against the percentage of extents of their lesions in each one of five subdivisions within the STS: MSTd, MSTl, MSTd plus MSTl, MT, and MSTd plus MSTl plus MT. Each monkey has two data entries in each of the graphs: the gray symbols showing the data when the extents of the lesions were based on the percentage of each subdivision that had been damaged partially or completely (i.e., the total lesion listed in Table 2) and the black symbols showing the data when the extents of the lesions were based only on the percentage of each subdivision in which the damage was complete. These plots indicate that there was a general tendency for the average OFR deficit to covary with both estimates of the percentage of extent of the morphological damage in the various subdivisions of the STS. However, the magnitude of the deficit in monkey P, which had previously been used for recordings in the NOT and the DLPN, was markedly greater than expected from the size of its cortical lesions and the data from the other four monkeys (Fig. 5, open inverted triangles). When the data from monkey P were excluded, linear regressions of these average OFR deficits on the extent of the lesions in each of the various subgroupings within the STS always showed significant positive slopes, with $r^2$ values ranging from 0.51 to 0.78 when based on the total extent of the lesions (Fig. 5, gray data and lines) and from 0.57 to 0.91 when based only on the extent of the complete lesions (Fig. 5, black data and lines). [Note that both parameters in these regressions, the magnitude of the OFR deficits ($Y$) and the extent of the lesions ($X$), were dependent variables, and to take into account the variance of $X$ as well as $Y$, the slopes given in Fig. 5 are the geometric means of the slope of $Y$ on $X$ and 1/(slope of $X$ on $Y$).] The positive correlation between the size of the lesion and the magnitude of the deficit was greatest for the complete lesions in MSTl.

### DVRs

Before the ibotenic acid injections, horizontal disparity steps applied to large-field, correlated, random-dot patterns elicited initial DVRs that were, in all essentials, like those described by previous authors (Busettini et al., 1996, 2001; Masson et al., 1997; Takemura et al., 2001) with onset latencies of 55–60 ms and mean

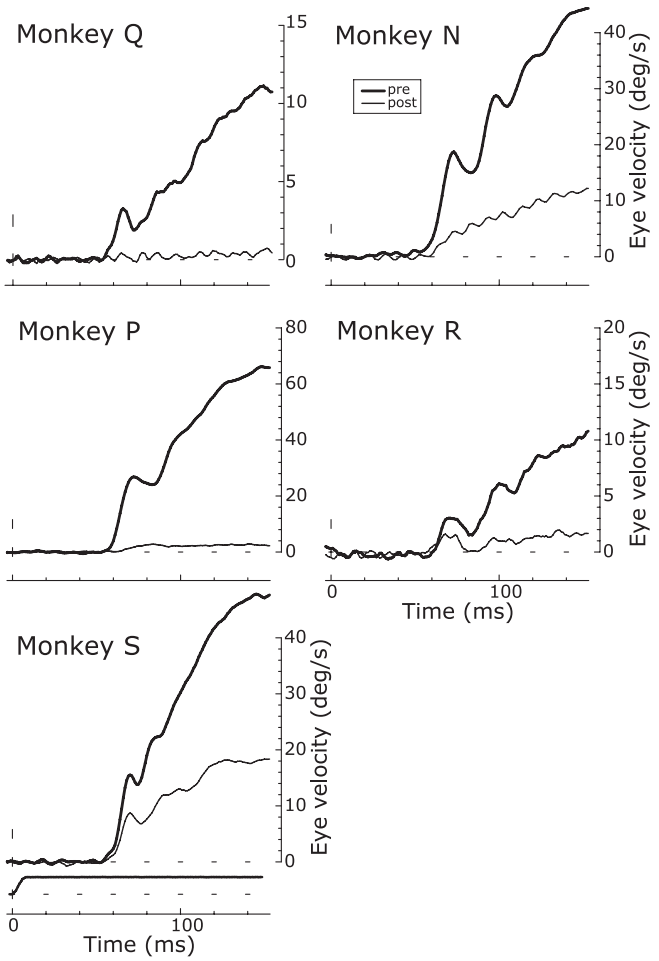


**Figure 2.** Deficits in OFRs after ibotenic acid injections: sample temporal profiles (data for each of the five monkeys). Mean eye velocity (in degrees per second) over time (in milliseconds) in response to multiple presentations of 80°/s downward ramps before (thick traces) and after (thin traces) the injections is shown. Upward deflections denote downward eye movements. The bottom left panel also includes the stimulus velocity profile.

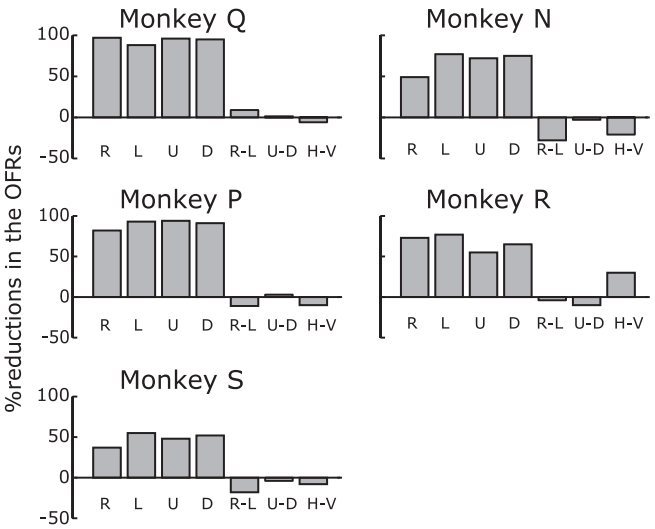


**Figure 3.** Deficits in OFRs after ibotenic acid injections (histograms for each of the five monkeys). R, L, U, and D, The percentage of reductions in the OFRs (based on the changes in eye position over the time period 50–100 ms) to rightward, leftward, upward, and downward motion, respectively, averaged for five speeds ranging from 10 to 160°/s; R-L, U-D, and H-V, differences between the mean percentage reductions to rightward and leftward, upward and downward, horizontal (R plus L), and vertical (U plus D), respectively.

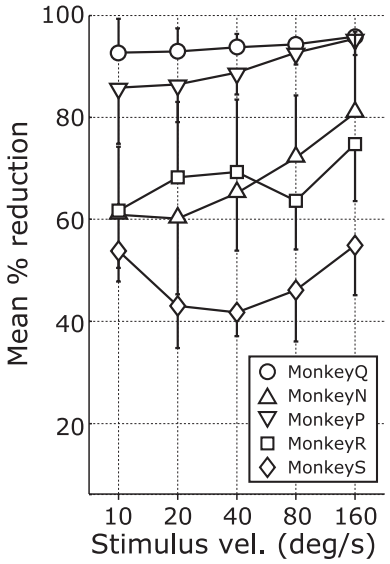


**Figure 4.** Deficits in OFRs after ibotenic acid injections: dependence on stimulus speed (data for each of the five monkeys). Ordinate, Percentage of reduction in the OFRs for each monkey, based on the mean changes in eye position (in degrees; over the time period 50–100 ms measured from onset of the stimulus ramps) averaged for all four cardinal directions. Abscissa, Stimulus speed (in degrees per second). Error bars indicate 1 SD. ○, Monkey Q; △, monkey N; ▽, monkey P; □, monkey R; ◇, monkey S. vel., Velocity.

vergence velocity profiles that showed an initial transient followed by a smaller sustained response (Fig. 6, thick traces), which show the convergent responses to 1° crossed-disparity steps (*A*) and the divergent responses to 1° uncrossed-disparity steps (*B*) for monkey N. In addition, disparity tuning curves, describing the dependence of the change-in-vergence-position measures (for the time period 50–100 ms from stimulus onset) on the amplitude of the disparity steps, approximated the derivative of a Gaussian, showing a central servo range over which crossed disparities resulted in convergent responses and uncrossed disparities resulted in divergent responses (Fig. 7, filled symbols). This servo range was quite narrow, and responses peaked with disparities of <2° before declining back to a non-zero asymptote as disparities exceeded ~4°, the so-called "default" response to uncorrelation (Busettini et al., 1996, 2001). The disparity tuning curves were fitted with the following equation from Busettini et al. (2001):

$$A\left[1 - e^{\frac{-|d|}{B}}\right] + G\exp\left[-\frac{(d-D)^2}{2\sigma^2}\right]\cos\left[2\pi f(d-D) + \phi\right]. \quad (1)$$

The first term in Equation 1 accounts for the non-zero asymptote and is an exponential function with an asymptotic level, *A*, and a space constant, *B*. The value of *B* was fixed at 0.46, based on the space constants found by Busettini et al. (2001) using the orthogonal responses to vertical disparity steps. The second term in Equation 1 is a Gabor function, in which $\sigma$ is the Gaussian width, *f* and $\phi$ are the spatial frequency and phase of the cosine term, and *G* is a gain factor. Because the data were usually not symmetrical about zero, we incorporated a parameter, *D*, to allow the peak of the Gaussian to shift (cf. Busettini et al., 2001). It is clear from Figure 7 that Equation 1 provided a good fit to our preinjection

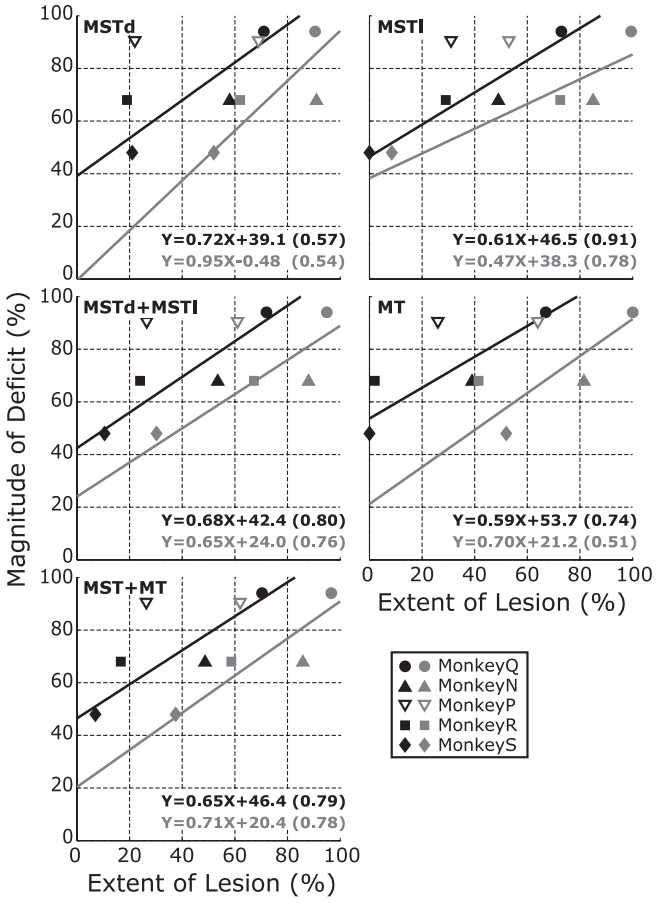


**Figure 5.** Deficits in OFRs after ibotenic acid lesions: dependence on the estimated extent of the lesions in MSTd, MSTl, and MT (data for each of the five monkeys). Ordinates, Percentage of reduction in the OFRs for each monkey, based on the mean changes in eye position (in degrees; over the time period 50–100 ms measured from onset of the stimulus ramps) averaged over all stimulus directions and speeds. Abscissas, Percentage of each designated subregion of the STS showing morphological damage in any layer (gray symbols, complete plus partial lesions) or all layers (black symbols, complete lesions). Lines are best-fit linear regessions (taking into account the variance of both *X* and *Y*), the coefficients of which are shown at the bottom right in each panel (the coefficients of determination are in parentheses). Data in open symbols (monkey P) were excluded from the regressions.

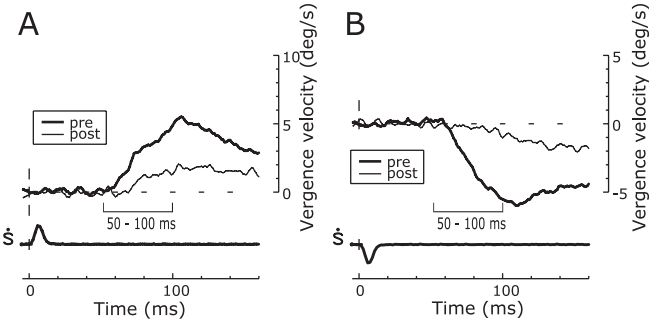


**Figure 6.** Deficits in DVRs after ibotenic acid injections: sample temporal profiles (monkey Q). Mean vergence velocity (in degrees per second) over time (in milliseconds) in response to multiple presentations of 1° crossed (***A***) and uncrossed (***B***) disparity steps before (pre; thick traces) and after (post; thin traces) the injections. Disparity steps were applied at zero on the time scale. Upward deflections denote convergent eye movements. The time bars, 50–100 ms, indicate the period over which the response measures were made.

data (closed symbols, continuous lines), and the best-fit parameters for these curves are listed in Table 3 (Pre), together with an estimate of the goodness of fit ($r^2$), the values of which ranged from 0.96 to 0.99.

After bilateral injections of ibotenic acid in the STS, there was a significant attenuation of the DVRs to many crossed- and uncrossed-disparity steps (Student's *t* test, $p < 0.05$) (Figs. 6, thin traces, 7, open symbols with an asterisk). The disparity tuning curves had the same general form after the injections as before and were again well fitted by Equation 1 (Fig. 7, dashed lines), with $r^2$ values ranging from 0.92 to 0.96; the best-fit parameters are listed in Table 3 (Post). The impact of the injections is perhaps best appreciated from the changes in the peak-to-peak amplitudes ($A_{p\text{-}p}$) of the best-fit curves in Figure 7, which are also listed in Table 3. The percentage of reductions in $A_{p\text{-}p}$ after the injections, which are given at the bottom right of each graph in Figure 7, averaged 58.6% (range, 36–79%) and were often correlated with the extent of the morphological damage in the various subdivisions of the STS. This can be seen in Figure 8, in which the percentage of reductions in $A_{p\text{-}p}$ are plotted against the percentage of extents of the lesions in the five subregions within the STS and which is organized exactly like Figure 5. Once again, monkey P (Fig. 8, open symbols) was an outlier with a greater deficit than expected from the size of its lesions, and when its data were excluded, linear regressions of the reductions in $A_{p\text{-}p}$ on the extent of the lesions in each of the various subdivisions of the STS always showed significant positive slopes, with $r^2$ values ranging from 0.63 to 0.84 when based on the total extent of the lesions (Fig. 8, gray symbols and lines) and from 0.69 to 0.94 when based only on the extent of the complete lesions (Fig. 8, black symbols and lines). The correlation between the size of the lesion and the magnitude of the deficit was greatest for the complete lesions in MSTl (compare the OFR). It is also very interesting that there was a highly significant correlation between the magnitudes of the OFR and DVR deficits documented in Figures 5 and 8 (correlation coefficient of 0.998 when data from monkey P were excluded).

### RFVRs

Radial-flow steps applied to large-field random-dot patterns generally elicited vergence eye movements at short latency that were, in all essentials, like the RFVRs described by previous authors (Busettini et al., 1997; Inoue et al., 1998b; Yang et al., 1999): transient convergent responses to expanding (centrifugal) steps and transient divergent responses to contracting (centripetal) steps with onset latencies of 60–70 ms. Sample temporal response profiles (means) obtained from monkey P with 5% steps can be seen in Figure 9 (thick traces); the data obtained with expansions are shown in *A*, and the data obtained with contractions are shown in *B*. However, response amplitudes were small (the peak eye velocity was often <2°/s) and in two cases, monkey R with centrifugal steps and monkey S with centripetal steps, failed to reach our response criterion (twice the SD of the baseline noise). The ibotenic acid injections in the STS always resulted in significant attenuation of the RFVRs, and this was so severe in the cases illustrated in Figure 9 that it is difficult to distinguish the postinjection responses (thin traces) from the baseline noise. The prelesion and postlesion RFVRs were assessed quantitatively using the change in vergence position over the time period 50–100 ms from stimulus onset, and these measures are listed in Table 4, together with the percentage of reduction in these measures resulting from the lesions (two rightmost columns). The reductions in the RFVRs after the injections ranged from 51 to 125% (mean reduction, 84%), and all were statistically significant (Student's *t* test, $p < 0.05$). (Reductions exceeding 100% indicate

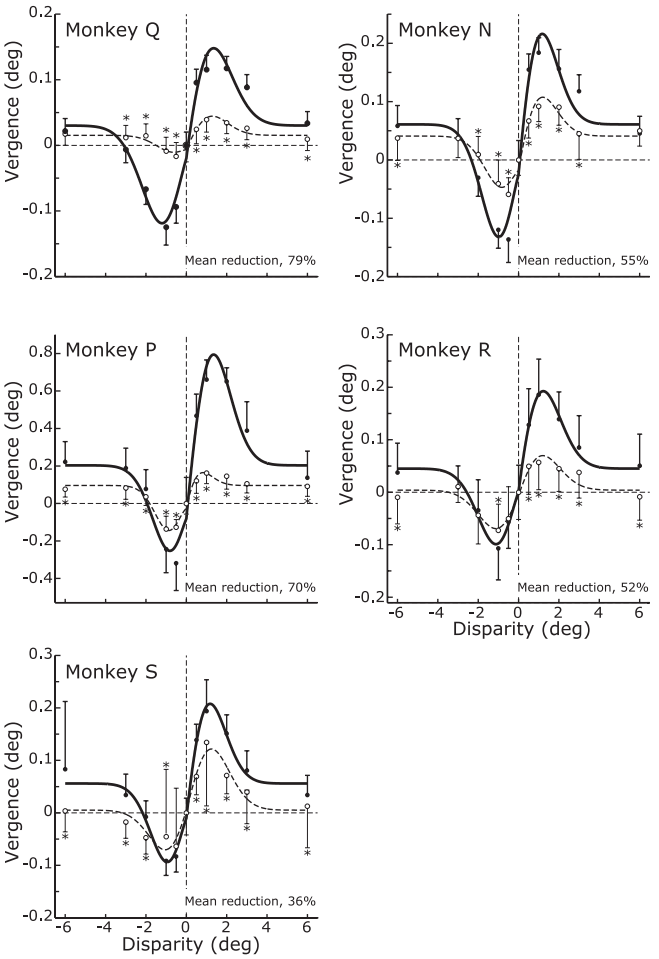


**Figure 7.** Deficits in DVRs after ibotenic acid injections: disparity tuning curves (data for each of the five monkeys). Ordinates, Vergence responses, based on the mean changes in horizontal vergence position (in degrees; over the time period 50–100 ms measured from onset of the disparity step) before (closed symbols) and after (open symbols) the injections. Abscissas, Disparity step (in degrees). Curves are the least-squares best fits obtained using Equation 1, and the data given at the bottom right in each panel are the mean percentage reductions in $A_{p\text{-}p}$ (peak-to-peak amplitude) based on values in Table 3. Error bars indicate 1 SD. *$p < 0.05$, postinjection data.

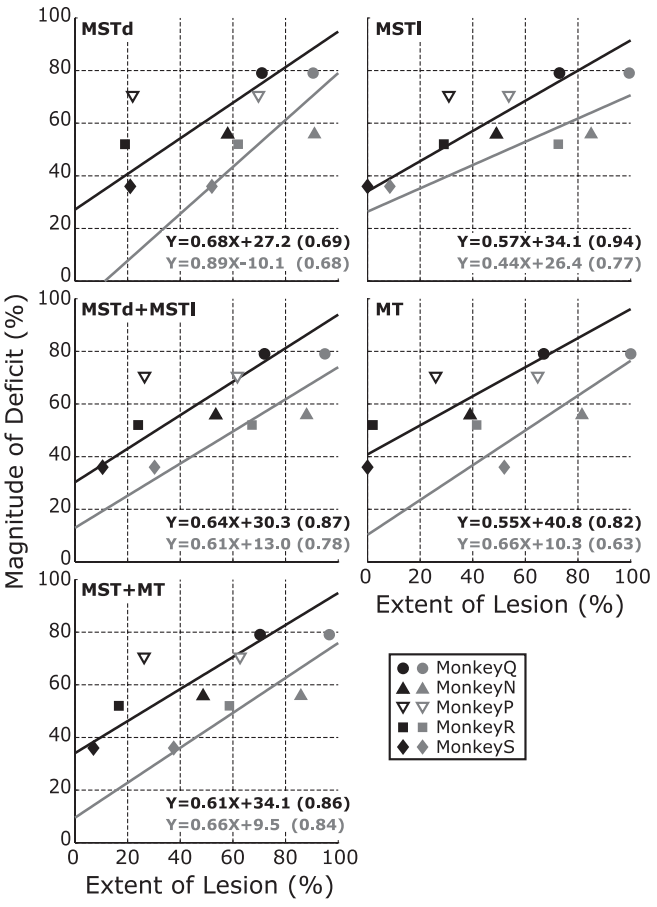


**Figure 8.** Deficits in DVRs after ibotenic acid lesions: dependence on the estimated extent of the lesions in MSTd, MSTl, and MT (data for each of the five monkeys). Ordinates, Percentage reduction in the DVRs for each monkey, based on the changes in the peak-to-peak amplitudes ($A_{p\text{-}p}$) of the least-squares best fits obtained with Equation 1 shown in Figure 7 (the parameters are listed in Table 3). Abscissas, Percentage of each designated subregion of the STS showing morphological damage in any layer (gray symbols, complete plus partial lesions) or all layers (black symbols, complete lesions). Lines are best-fit linear regessions (taking into account the variance of both *X* and *Y*), the coefficients of which are shown at the bottom right in each panel (coefficients of determination are in parentheses). Data in open symbols (monkey P) were excluded from the regressions.

response reversal, but we assume that these reversals probably reflected noise, given that even the preinjection responses were very small.) The magnitude of these lesion effects was poorly correlated with the extent of the damage in the various subdivisions of the STS, whether considering all areas affected by the lesion (total lesion) or only the areas with complete lesions, and the $r^2$ values never exceeded 0.18. Unfortunately, the marginal amplitude of the RFVRs even before the injections raises the possibility that noise obscured any relationship between the magnitude of the deficits and the size of the lesions in the various subregions. In addition, noise might have been a major factor in our finding that there was no significant correlation between the RFVR deficits and the deficits in the OFR and DVR documented in Figures 5 and 8 (correlation coefficients of 0.114 and 0.115, respectively, when data from monkey P were excluded).

### Optokinetic and smooth-pursuit eye movements

Optokinetic and smooth-pursuit eye movements were recorded in two monkeys (P and S) before and after the ibotenic acid injections. Before injection, optokinetic nystagmus (OKN) was as described by previous authors (Cohen et al., 1977; Lisberger et al., 1981): slow-phase eye velocity showed an initial rapid rise (OKNe) and, if eye speed fell short of stimulus speed at the end of this phase, was followed by a more gradual buildup in eye speed (OKNd); after the stimulus was blanked, slow-phase eye velocity showed an initial rapid drop, followed by a more gradual decline as eye speed slowly fell back toward zero (OKAN). This pattern of responses is evident in the sample data shown in Figure 10, *A* and *B*, that were obtained from monkey P before the ibotenic acid injections. There is substantial evidence (for review, see Lisberger et al., 1981) indicating that the optokinetic responses are generated by two neural mechanisms, one with brisk dynamics that is responsible for the rapid changes in slow-phase eye velocity (OKNe and the rapid drop after blanking) and the other with sluggish dynamics that is responsible for the more gradual changes (OKNd and OKAN). A previous study showed that both of these components were reduced to varying degrees by unilateral chemical lesions in MST (Dürsteler and Wurtz, 1988): the slow buildup was impaired only for motion toward the side of the lesion, and the initial rapid rise was impaired for motion toward or away from the side of the lesion. Our observations were consistent with this, as indicated by the sample data shown in Figure 10, *C* and *D*, that were obtained from monkey P after bilateral

**Table 3. Dependence of the mean DVRs on the magnitude of the disparity steps before and after the ibotenic acid injections: best-fit parameters when the data were fitted with Equation 1**

| | | $A$ | $G$ | $\sigma$ | $D$ | $f$ | $\phi$ | $A_{p\text{-}p}$ | $r^2$ |
|---|---|---|---|---|---|---|---|---|---|
| | Pre | 0.03 | 1.24 | 1.29 | −0.017 | 0.022 | 269.0 | 0.27 | 0.97 |
| Monkey Q | Post | 0.02 | 0.40 | 1.02 | 0.307 | 0.017 | 270.9 | 0.06 | 0.92 |
| | Pre | 0.06 | 2.53 | 1.09 | 0.012 | 0.017 | 269.5 | 0.35 | 0.96 |
| Monkey N | Post | 0.04 | 0.14 | 1.26 | 0.042 | 0.138 | 264.4 | 0.16 | 0.95 |
| | Pre | 0.20 | 6.97 | 1.12 | 0.307 | 0.017 | 271.2 | 1.05 | 0.97 |
| Monkey P | Post | 0.10 | 0.63 | 0.82 | −0.310 | 0.077 | 258.8 | 0.31 | 0.96 |
| | Pre | 0.05 | 1.88 | 1.18 | 0.038 | 0.017 | 270.3 | 0.29 | 0.99 |
| Monkey R | Post | 0.00 | 0.68 | 1.17 | 0.001 | 0.023 | 269.5 | 0.14 | 0.92 |
| | Pre | 0.06 | 1.87 | 1.08 | 0.094 | 0.020 | 270.3 | 0.30 | 0.98 |
| Monkey S | Post | 0.01 | 1.39 | 1.15 | 0.220 | 0.016 | 271.4 | 0.19 | 0.94 |

An iterative procedure with a least-squares criterion was used to obtain the best fits with each of the parameters resolved to the number of decimal places shown. $A_{p\text{-}p}$ is the peak-to-peak amplitude of Equation 1. $r^2$ is the coefficient of determination. $A$, $D$, $G$, $\sigma$, $\phi$, and $A_{p\text{-}p}$ are in degrees, and $f$ is in cycles/degree. Disparity tuning curves based on these best-fit parameters are shown in Fig. 7. Pre, Preinjection data; Post, postinjection data.

ibotenic acid injections: the brisk responses were severely attenuated to both rightward and leftward motion, whereas the sluggish responses were only impaired with the leftward motion (Fig. 10*D*), perhaps reflecting our finding that the total extent of the lesion in the left MSTl was about twice that in the right MSTl in this animal (Table 2). However, a complication here is that monkey P had been used for previous recordings in the left NOT, which might normally contribute to the slow buildup response to the leftward motion. The initial eye acceleration, based on the change in eye velocity over the first 100 ms of the response, which is a measure of the brisk component, was reduced in monkey P by 74 ± 34% ($n = 3$) and 99 ± 8% ($n = 3$) with rightward and leftward motion, respectively; these reductions were 18 ± 17% ($n = 3$) and 56 ± 21% ($n = 3$) in monkey S. The average velocity of the last five slow phases of the OKN (the final OKN), which is a measure of the combined effects of the brisk and sluggish components, was reduced after the injections in monkey P by 11 ± 17% ($n = 3$) and 73 ± 12% ($n = 3$) with the rightward and leftward motion, respectively, but showed little change in monkey S, with the corresponding changes of −5 ± 10% ($n = 3$) and 1 ± 6% ($n = 3$), respectively. The effect of the injections on the average velocity of the first three slow phases of the OKAN (the initial OKAN), which is a measure of the sluggish component, were more variable; only the responses of monkey P to leftward motion stimuli showed a reduction of 56 ± 14% ($n = 3$). All remaining measures of initial OKAN were increased after the lesion, by 70 ± 34% ($n = 3$) in monkey P with rightward motion and by 87 ± 35% ($n = 3$) and 71 ± 18% ($n = 3$) in monkey S with rightward and leftward motion, respectively. Nonetheless, the rapid drop in eye velocity after blanking [(1 − (initial OKAN/final OKN)) × 100%] was consistently smaller after the injections by 72 ± 12% ($n = 3$) and 44 ± 41% ($n = 3$) in monkey P with rightward and leftward motion, respectively, and by 70 ± 21% ($n = 3$) and 44 ± 12% ($n = 3$) in monkey S with rightward and leftward motion, respectively.

Previous studies that placed chemical lesions in MST and/or MT of one hemisphere reported two types of deficits in the pursuit eye movements elicited by discrete moving targets: impaired initiation of pursuit to target motion in any direction and impaired maintenance of pursuit when the target motion was toward the side of the lesion (Newsome et al., 1985; Dürsteler et al., 1987; Dürsteler and Wurtz, 1988; Yamasaki and Wurtz, 1991). We too observed significant deficits in the initiation and maintenance of pursuit after bilateral chemical lesions in STS, as can be seen in Figure 11*A*, which shows sample preinjection (thick traces) and postinjection (thin traces) response profiles obtained from monkey P with 20°/s leftward and rightward target motion. However, the deficits were often quite modest. This is evident from the percentage of reduction in our quantitative measures of the presaccadic and postsaccadic tracking (based on the changes in eye position over the time intervals 100–150 ms and 300–350 ms, respectively, measured from the onset of target motion), which are plotted separately for monkeys P and S in Figure 11*B*.

### Other oculomotor parameters

After ibotenic acid injections in the STS of one hemisphere, all monkeys showed a mild nystagmus when placed in the dark, with slow phases directed away from the side of injection. After injections in both hemispheres, a nystagmus was still evident in the dark, but now it was vertical in four monkeys (upward slow phases in monkeys Q, P, and R; downward slow phases in monkey N) and rightward in monkey S. However, in all cases, the nystagmus was primarily suppressed when monkeys viewed the stationary random-dot test patterns. This was evident from the ocular drift speeds averaged over the critical 50 ms time period commencing with the onset of the OFR stimuli (vertical eye movements were recorded only in the OFR paradigm, so only in this paradigm were we able to assess the true ocular drift speed, and then only for the right eye), the mean values of which are plotted for all subjects in Figure 12*A*. Another important point is that only in one monkey (Q) was the mean ocular drift speed increased significantly after the injections, and then by only a small amount, 0.6°/s. In two monkeys (P, R), the mean drift speed (and its variance) were actually slightly lower after the injections.

After the injections, the centering saccades showed very modest increases in amplitude and peak velocity in four of five monkeys, and these were generally statistically significant (see the average data for each of the five monkeys plotted in Figure 12*B*,*C*). The "prelesion minus postlesion" differences in the average amplitudes and peak velocities ranged from −1.4 to 0.3° and from −76 to 21°/s, respectively. A related concern is how well the stimulus patterns were centered on the retina when the stimuli were applied, and this was checked by measuring the angular distance between the fovea and the screen center ("retinal eccentricity") during the 50 ms time period starting with the onset of the stimulus. In the OFR paradigm, estimated retinal eccentricities were actually slightly smaller for three of five monkeys after the injections (mean reduction of 0.9° in those monkeys), and the increases in the other two monkeys amounted to only 0.1 and 0.7°(Fig. 12*D*). After the injections, four of five monkeys showed small (0.1–0.3°) but statistically significant changes in the mean vergence error during the 50 ms time period starting with the onset of the stimuli (Fig. 12*E*). However, only in one case (monkey R) did this result in an increase in the mean vergence error.

## Discussion

### A family of short-latency reflexes mediated by the STS

Bilateral ibotenic acid injections in the STS of five monkeys caused morphological changes in the three subregions (MSTd, MSTl, and MT) and resulted in significant deficits in the initial OFRs, DVRs, and RFVRs of all animals. We also examined OKN and pursuit eye movements in two of the monkeys and, in line with previous studies that lesioned MT and MST (Newsome et

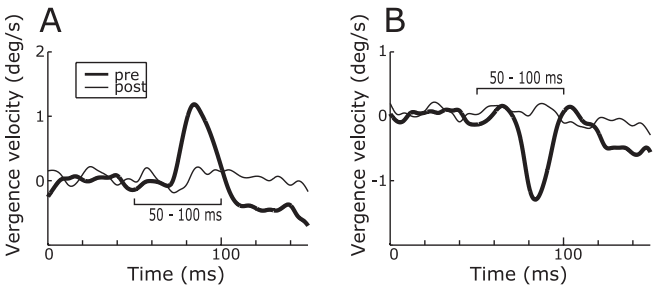


**Figure 9.** Deficits in RFVRs after ibotenic acid injections: sample temporal profiles (monkey P). Mean horizontal vergence velocity (in degrees per second) over time (in milliseconds) in response to multiple presentations of 2% expansions (***A***) and contractions (***B***) before (pre; thick traces) and after (post; thin traces) the injections. Radial flow steps were applied at zero on the time scale. Upward deflections denote convergent eye movements. The time bars, 50–100 ms, indicate the period over which the response measures were made.

al., 1985; Dürsteler et al., 1987; Dürsteler and Wurtz, 1988; Yamasaki and Wurtz, 1991), observed significant deficits in both types of tracking. The magnitudes of the deficits in the OFR and DVR in a given animal were directly related to the percentage of extent of the morphological damage in the three subregions of the STS (Figs. 5, 8) (excluding the data from monkey P). In fact, the correlation between the size of the lesion and the magnitude of the deficit in the OFR and DVR was highest for MSTl ($r^2 = 0.91$ and 0.94, respectively). However, the percentage of extent of the lesions in the three subregions often covaried, rendering the relative contribution of any given subregion to the various deficits uncertain. Notably, it is not possible to attribute any particular deficit solely to damage in one particular subregion. Furthermore, we are unable to determine whether the cortical regions that sustained only partial damage contributed to the deficits. Yet another potential complication is that others who have used ibotenic acid injections in STS presented evidence suggesting that "the area affected by the injection might be somewhat larger than indicated by the area of cell death" (Dürsteler et al., 1987). These reservations notwithstanding, insofar as MST sustained significant morphological damage in all injected hemispheres, our findings are consistent with our previous suggestions that neurons in MST have a causal role in the genesis of all three kinds of reflex eye movements. However, we must also concede that the damage to MT might have contributed significantly to the observed deficits, not the least because MT is a major source of inputs to MST (Maunsell and van Essen, 1983b; Ungerleider and Desimone, 1986). The deficits in the DVR and the OFR were highly correlated, consistent with a common distributed organization within the STS, although the former were generally less severe than the latter, perhaps suggesting that the DVR is more heavily reliant on other cortical areas. As already pointed out, the marginal amplitude of the RFVRs even before the injections means that noise might have obscured any clear relationship between the RFVR deficits and the size of the lesions or the deficits in the other two reflexes.

**Secondary effects?**

A major concern was the possibility that these deficits might be secondary to deficits in other aspects of the monkeys' oculomotor performance that are known to be critical for the normal functioning of the three reflexes.

*Postsaccadic enhancement*

All test stimuli were applied in the immediate wake of a centering saccade to take advantage of postsaccadic enhancement (Kawano and Miles, 1986; Busettini et al., 1996, 1997), and there is evidence that MST contributes to this enhancement, at least in the case of the OFR (Takemura and Kawano, 2006). If the STS lesions reduced this enhancement, then this alone would be expected to reduce the gain of the responses. In addition, the postsaccadic enhancement of the OFR and DVR is known to be attributable in part to the visual reafference caused by the antecedent saccade sweeping the image of the background across the retina (Kawano and Miles, 1986; Busettini et al., 1996); therefore, any effects of the lesions on the speed and amplitude of the centering saccades might also have had an impact on the magnitude of this visual reafference and the associated enhancement. Previous studies reported that STS lesions had little impact on saccades to stationary targets (Newsome et al., 1985; Dürsteler and Wurtz, 1988). The centering saccades in the present study were, on average, slightly larger and faster in four of five monkeys after the lesions (Fig. 12*B*,*C*), and the study by Kawano and Miles (1986) on the OFR suggests that this would actually work to increase the component of the postsaccadic enhancement of the OFR because of visual reafference, albeit only slightly. No quantitative information is available regarding the dependence of the postsaccadic enhancement of the DVR and the RFVR (or the nonvisual component of the postsaccadic enhancement of the OFR) on the parameters of the saccade. However, we think it unlikely that these factors made more than a minor contribution to the observed impairments of the three tracking mechanisms, and they might even have had the converse effect.

*Retinal eccentricity*

The slight changes in the amplitudes of the centering saccades raise another potential concern: How well were the stimulus patterns centered on the retina when the stimuli were applied? Given the large size of the stimulus patterns ($90 \times 90°$), we think it very unlikely that the slight, inconsistent changes in the retinal eccentricity after the injections (ranging from a decrease of 1.2° to an increase of 0.7°) would have had much impact on the OFRs or DVRs. In the case of the OFR, it is known that the major visual drive comes from the central 40° of the visual field (Miles et al., 1986). A recent study on humans indicated that increasing the retinal eccentricity of the focus of expansion/contraction reduced the magnitude of the RFVR at most 5% per degree (Miles et al., 2004). If we assume that the situation is very similar in the monkey and also that the retinal eccentricity during the RFVR experiments was similar to that during the OFR experiments (Fig. 12*D*), then we can estimate the likely impact on the RFVRs. The estimated postsaccadic eccentricity of gaze was actually reduced after the lesions in monkeys Q, R, and S by 1.1, 0.3, and 1.2°, respectively (which would work to increase the RFVR at most by 5.5, 1.5, 6%, respectively), and increased in monkeys N and P by 0.1 and 0.7°, respectively (which would work to decrease the RFVR at most by 0.5 and 3.5%, respectively).

*Postsaccadic drift*

The effects of the lesions on the ocular drift during the time the stimuli were being applied were invariably minor (Fig. 12*A*). Only monkey Q showed a significant increase, and this was very small (mean increase, 0.6°/s). This might have made a very minor contribution to the unusually large deficits seen in this monkey.

*Vergence errors and fixation disparity*

The OFR is known to be sensitive to binocular disparity (Takemura et al., 2000; Masson et al., 2001; Yang and Miles, 2003) and so would be influenced by any effect of the lesions on the vergence error such as those documented in Figure 12*E*. In addition, the

**Table 4. The vergence responses to expanding and contracting radial optic flow before and after the ibotenic acid injections**

| | Prelesion | | Postlesion | | Percentage of reduction | |
|---|---|---|---|---|---|---|
| | Expand | Contract | Expand | Contract | Expand | Contract |
| Monkey Q | +14.8 | −4.5 | +1.0 | −0.9 | +93** | +80** |
| Monkey N | +13.9 | −11.7 | +6.8 | −4.7 | +51* | +60** |
| Monkey P | +19.3 | −19.3 | +2.2 | +4.9 | +89** | +125** |
| Monkey R | | −26.0 | | +4.2 | | +116** |
| Monkey S | +41.1 | | +18.9 | | +54** | |

The prelesion and postlesion entries are the change-in-vergence position measures (over the time period 50–100 ms from stimulus onset) in degrees × $10^{-3}$; a positive sign indicates convergence, and a negative sign indicates divergence. Blank entries indicate that the response failed to exceed twice the SD of the baseline noise. Reductions exceeding 100% indicate reversal of the RFVR. *$p < 0.05$; **$p \leq 0.001$.

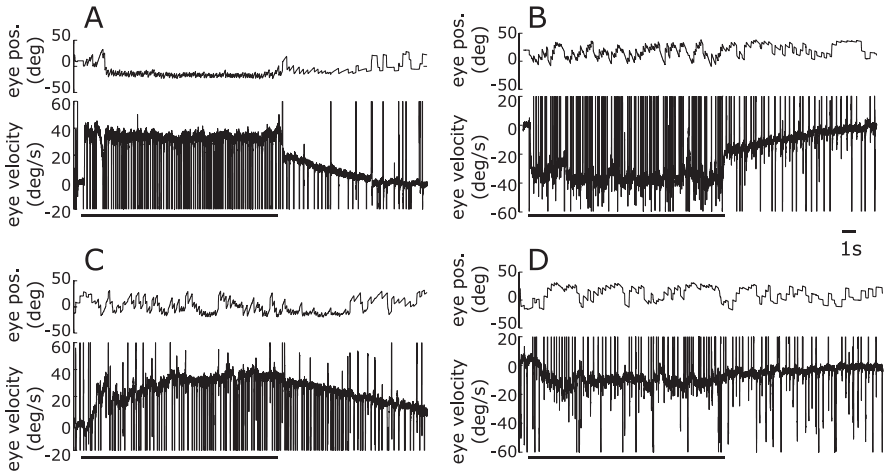


**Figure 10.** Deficits in the optokinetic responses after ibotenic acid injections: sample temporal profiles (monkey P). ***A***, ***B***, Data obtained before the injections. ***C***, ***D***, Data obtained after the injections. In each panel, the top traces show horizontal eye position (eye pos.; in degrees), and the bottom traces show horizontal eye velocity (in degrees per second) over time (in milliseconds) in response to rightward (***A***, ***C***) and leftward (***B***, ***D***) motion of a random-dot pattern at 40°/s. Upward deflections denote eye movements in the direction of stimulus motion. Thick lines indicate the duration of the illumination of the already-moving random-dot pattern.

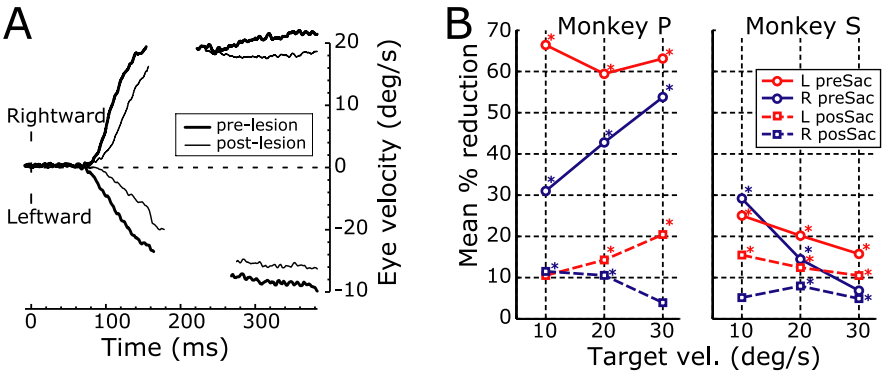


**Figure 11.** Deficits in smooth-pursuit eye movements after ibotenic acid injections: sample temporal profiles (monkey P) and response measures (monkeys P and S). ***A***, Mean eye velocity (in degrees per second) over time (in milliseconds) in response to multiple presentations of 20°/s leftward and rightward ramps before (pre; thick traces) and after (post; thin traces) the injections; upward deflections denote rightward eye movements, and gaps are attributable to deletions of saccadic intrusions. ***B***, Percentage of reductions in the pursuit responses, based on the mean changes in eye position over (1) the time period 100–150 ms (continuous lines: presaccadic, open-loop responses) and (2) the time period 300–350 ms (dashed lines: postsaccadic, closed-loop responses), both measured from the onset of the stimulus ramps. Red, Leftward ramps; blue, rightward ramps; abscissa, stimulus speed (in degrees per second). vel., Velocity; L, left; R, right; preSac, presaccadic; posSac, postsaccadic.

gain of the OFR is known to be directly dependent on the vergence angle, independent of binocular disparity (Busettini et al., 1991; Inoue et al., 1998a). Based on the measured vergence angle for every trial, we estimated that the effect of the lesions on fixation disparity [the dependence of the OFR on disparity was known for monkeys Q, P, and N because they had been subjects in the study by Takemura et al. (2000); for monkeys R and S, we used the data from the other three monkeys to estimate a mean curve describing dependence of the OFR on disparity] and vergence angle [we assumed a mean sensitivity of 10% per degree (Inoue et al., 1998a)] per se would have operated to decrease the OFR of monkeys Q and P, on average, by 18 and 15%, respectively, and increase the OFR of monkeys N, R, and S, on average, by 1, 16, and 3%, respectively. A recent study on humans reported that the amplitude of the initial RFVR was linearly dependent on the vergence angle with an average sensitivity of 15%/$m^{-1}$ for expanding flow and 22%/$m^{-1}$ for contracting flow (Yang et al., 1999). If we assume that the monkey's RFVR has a similar dependence, then based on the measured vergence angle for every trial, we estimated that the effect of the lesions on vergence angle would have operated to decrease the RFVR of monkeys Q and S, on average, by 2.0 and 1.3%, respectively, and increase the RFVR of monkeys P and R, on average, by 1.8 and 2.8%, respectively. It is not known whether the RFVR is sensitive to binocular disparity, although it is known to be driven very successfully by monocular stimuli (Busettini et al., 1997). The slight effects of the STS lesions on the fixation disparity would be expected to result in an offset in the disparity steps used to elicit the DVR and hence might be expected to cause slight horizontal shifts without influencing the general form and amplitude of the disparity tuning curves like those in Fig. 7.

We conclude that most of the deficits in the OFR, DVR, and RFVR after ibotenic acid injections in the STS were primary and not secondary to changes in other oculomotor parameters such as postsaccadic enhancement, ocular drift, vergence errors, or fixation disparity.

### Population coding and multiplexing

In a recent study, we showed that the summed activity of the disparity-sensitive cells in MST effectively encodes the initial DVR although there is no hint of this vergence information at the level of the individual cells, indicating that the representation of the DVR in MST is an "emergent property" of the overall activity: population coding (Takemura et al., 2001, 2002b). Quantitative analyses indicated that the projection from MST to the next stage in the processing of the vergence drive signal must include contributions from the full spectrum of disparity-selective cells and raised

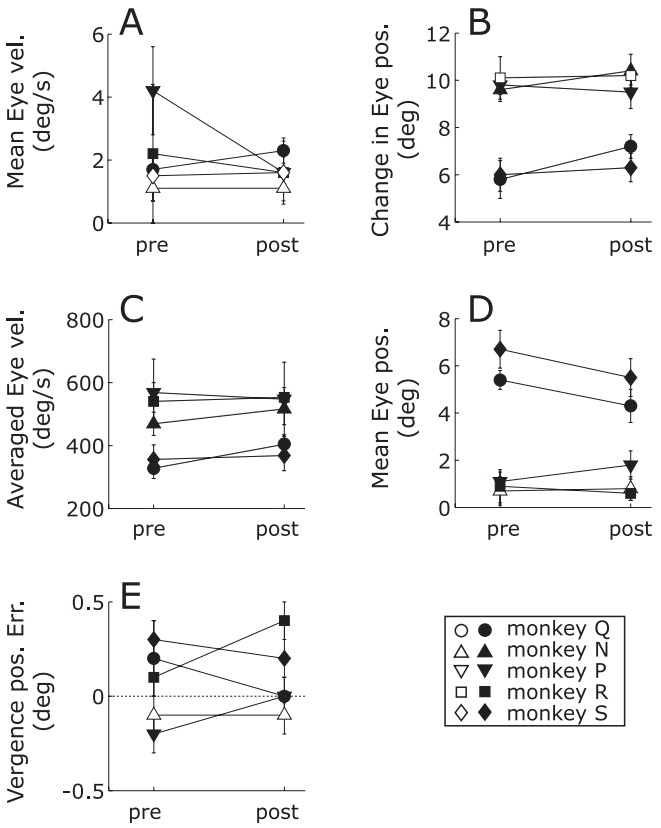


**Figure 12.** General oculomotor characteristics before (pre) and after (post) ibotenic acid injections. ***A***, Mean ocular drift during the 50-ms period commencing with the onset of the visual stimulus; values are mean drift speeds in degrees per second (±1 SD) of the velocity vector. ***B***, Mean amplitude of the leftward-centering saccades in degrees (±1 SD). ***C***, Mean peak velocity of the leftward-centering saccades in degrees per second (±1 SD). ***D***, Mean eccentricity of gaze in degrees (±1 SD) in the OFR paradigm during the 50 ms period commencing with the onset of the visual stimulus. ***E***, Mean vergence error in degrees (±1 SD) in the RFVR paradigm during the 50 ms period commencing with the onset of the visual stimulus; a positive sign indicates overconvergence. Filled symbols denote that the differences between the means before and after the injections were statistically significant at the 0.05 level (Student's *t* test). vel., Velocity; pos., position; Err., error.

the possibility that it involves merely a random selection of those cells. That the DVR (and OFR) deficits in the present study involved a simple attenuation directly related to the size of the lesion is consistent with reliance on a randomly distributed population of disparity-selective (and motion-selective) cells. Unfortunately, no population data are yet available for the neurons in MST that are known to discharge in relation to the OFR (Kawano et al., 1994; Takemura et al., 2000) and the RFVR (our unpublished observations).

## References

Busettini C, Miles FA, Schwarz U (1991) Ocular responses to translation and their dependence on viewing distance. II. Motion of the scene. J Neurophysiol 66:865–878.

Busettini C, Miles FA, Krauzlis RJ (1996) Short-latency disparity vergence responses and their dependence on a prior saccadic eye movement. J Neurophysiol 75:1392–1410.

Busettini C, Masson GS, Miles FA (1997) Radial optic flow induces vergence eye movements with ultra-short latencies. Nature 390:512–515.

Busettini C, Fitzgibbon EJ, Miles FA (2001) Short-latency disparity vergence in humans. J Neurophysiol 85:1129–1152.

Cohen B, Matsuo V, Raphan T (1977) Quantitative analysis of the velocity characteristics of optokinetic nystagmus and optokinetic after-nystagmus. J Physiol (Lond) 270:321–344.

Desimone R, Ungerleider LG (1986) Multiple visual areas in the caudal superior temporal sulcus of the macaque. J Comp Neurol 248:164–189.

Duffy CJ, Wurtz RH (1991) Sensitivity of MST neurons to optic flow stimuli. I. A continuum of response selectivity to large-field stimuli. J Neurophysiol 65:1329–1345.

Dürsteler MR, Wurtz RH (1988) Pursuit and optokinetic deficits following chemical lesions of cortical areas MT and MST. J Neurophysiol 60:940–965.

Dürsteler MR, Wurtz RH, Newsome WT (1987) Directional pursuit deficits following lesions of the foveal representation within the superior temporal sulcus of the macaque monkey. J Neurophysiol 57:1262–1287.

Eifuku S, Wurtz RH (1999) Response to motion in extrastriate area MSTl: disparity sensitivity. J Neurophysiol 82:2462–2475.

Fuchs AF, Robinson DA (1966) A method for measuring horizontal and vertical eye movement chronically in the monkey. J Appl Physiol 21:1068–1070.

Gallyas F (1979) Silver staining of myelin by means of physical development. Neurol Res 1:203–209.

Inoue Y, Takemura A, Kawano K, Kitama T, Miles FA (1998a) Dependence of short-latency ocular following and associated activity in the medial superior temporal area (MST) on ocular vergence. Exp Brain Res 121:135–144.

Inoue Y, Takemura A, Suehiro K, Kodaka Y, Kawano K (1998b) Short-latency vergence eye movements elicited by looming step in monkeys. Neurosci Res 32:185–188.

Judge SJ, Richmond BJ, Chu FC (1980) Implantation of magnetic search coils for measurement of eye position: an improved method. Vision Res 20:535–538.

Kawano K, Miles FA (1986) Short-latency ocular following responses of monkey. II. Dependence on a prior saccadic eye movement. J Neurophysiol 56:1355–1380.

Kawano K, Shidara M, Watanabe Y, Yamane S (1994) Neural activity in cortical area MST of alert monkey during ocular following responses. J Neurophysiol 71:2305–2324.

Komatsu H, Wurtz RH (1988) Relation of cortical areas MT and MST to pursuit eye movements. I. Localization and visual properties of neurons. J Neurophysiol 60:580–603.

Lisberger SG, Miles FA, Optican LM, Eighmy BB (1981) Optokinetic response in monkey: underlying mechanisms and their sensitivity to long-term adaptive changes in vestibuloocular reflex. J Neurophysiol 45:869–890.

Masson GS, Busettini C, Miles FA (1997) Vergence eye movements in response to binocular disparity without depth perception. Nature 389:283–286.

Masson GS, Busettini C, Yang DS, Miles FA (2001) Short-latency ocular following in humans: sensitivity to binocular disparity. Vision Res 41:3371–3387.

Maunsell JH, Van Essen DC (1983a) Functional properties of neurons in middle temporal visual area of the macaque monkey. II. Binocular interactions and sensitivity to binocular disparity. J Neurophysiol 49:1148–1167.

Maunsell JH, van Essen DC (1983b) The connections of the middle temporal visual area (MT) and their relationship to a cortical hierarchy in the macaque monkey. J Neurosci 3:2563–2586.

Miles FA (1998) The neural processing of 3-D visual information: evidence from eye movements. Eur J Neurosci 10:811–822.

Miles FA, Kawano K (1986) Short-latency ocular following responses of monkey. III. Plasticity. J Neurophysiol 56:1381–1396.

Miles FA, Kawano K, Optican LM (1986) Short-latency ocular following responses of monkey. I. Dependence on temporospatial properties of visual input. J Neurophysiol 56:1321–1354.

Miles FA, Busettini C, Masson GS, Yang D-S (2004) Short-latency eye movements: evidence for rapid, parallel processing of optic flow. In: Optic flow and beyond (Vaina LM, Beardsley SA, Rushton S, eds), pp 79–107. Dordrecht, The Netherlands: Kluwer Academic.

Newsome WT, Wurtz RH, Dürsteler MR, Mikami A (1985) Deficits in visual motion processing following ibotenic acid lesions of the middle temporal visual area of the macaque monkey. J Neurosci 5:825–840.

Roy JP, Wurtz RH (1990) The role of disparity-sensitive cortical neurons in signalling the direction of self-motion. Nature 348:160–162.

Roy JP, Komatsu H, Wurtz RH (1992) Disparity sensitivity of neurons in monkey extrastriate area MST. J Neurosci 12:2478–2492.

Shidara M, Kawano K (1993) Role of Purkinje cells in the ventral paraflocculus in short-latency ocular following responses. Exp Brain Res 93:185–195.

Takemura A, Kawano K (2006) Neuronal responses in MST reflect the post-saccadic enhancement of short-latency ocular following responses. Exp Brain Res 173:174–179.

Takemura A, Inoue Y, Kawano K (2000) The effect of disparity on the very earliest ocular following responses and the initial neuronal activity in monkey cortical area MST. Neurosci Res 38:93–101.

Takemura A, Inoue Y, Kawano K, Quaia C, Miles FA (2001) Single-unit activity in cortical area MST associated with disparity-vergence eye movements: evidence for population coding. J Neurophysiol 85:2245–2266.

Takemura A, Inoue Y, Kawano K (2002a) Visually driven eye movements elicited at ultra-short latency are severely impaired by MST lesions. Ann NY Acad Sci 956:456–459.

Takemura A, Kawano K, Quaia C, Miles FA (2002b) Population coding in cortical area MST. Ann NY Acad Sci 956:284–296.

Tanaka K, Saito H (1989) Analysis of motion of the visual field by direction, expansion/contraction, and rotation cells clustered in the dorsal part of the medial superior temporal area of the macaque monkey. J Neurophysiol 62:626–641.

Tanaka K, Hikosaka K, Saito H, Yukie M, Fukada Y, Iwai E (1986) Analysis of local and wide-field movements in the superior temporal visual areas of the macaque monkey. J Neurosci 6:134–144.

Ungerleider LG, Desimone R (1986) Cortical connections of visual area MT in the macaque. J Comp Neurol 248:190–222.

Van Essen DC, Maunsell JH (1980) Two-dimensional maps of the cerebral cortex. J Comp Neurol 191:255–281.

Van Essen DC, Maunsell JH, Bixby JL (1981) The middle temporal visual area in the macaque: myeloarchitecture, connections, functional properties and topographic organization. J Comp Neurol 199:293–326.

Wurtz RH (1969) Visual receptive fields of striate cortex neurons in awake monkeys. J Neurophysiol 32:727–742.

Yamasaki DS, Wurtz RH (1991) Recovery of function after lesions in the superior temporal sulcus in the monkey. J Neurophysiol 66:651–673.

Yang D, Fitzgibbon EJ, Miles FA (1999) Short-latency vergence eye movements induced by radial optic flow in humans: dependence on ambient vergence level. J Neurophysiol 81:945–949.

Yang DS, Miles FA (2003) Short-latency ocular following in humans is dependent on absolute (rather than relative) binocular disparity. Vision Res 43:1387–1396.

Available online at www.sciencedirect.com
SCIENCE DIRECT®
Vision Research 46 (2006) 869–878
Vision Research
www.elsevier.com/locate/visres

# The visual motion detectors underlying ocular following responses in monkeys

Kenichiro Miura [a,b,*], Kiyoto Matsuura [b], Masakatsu Taki [b,c], Hiromitsu Tabata [a,b], Naoko Inaba [b], Kenji Kawano [b], Frederick A. Miles [d]

[a] *Horizontal Medical Research Organization, Graduate School of Medicine, Kyoto University, Japan*
[b] *Department of Integrative Brain Science, Graduate School of Medicine, Kyoto University, Japan*
[c] *Department of Otolaryngology, Kyoto Prefectural University of Medicine, Japan*
[d] *Laboratory of Sensorimotor Research, National Eye Institute, National Institutes of Health, USA*

Received 8 August 2005; received in revised form 20 October 2005

**Abstract**

Psychophysical evidence indicates that visual motion can be sensed by low-level (energy-based) and high-level (feature-based) mechanisms. The present experiments were undertaken to determine which of these mechanisms mediates the initial ocular following response (OFR) that can be elicited at ultra-short latencies by sudden motion of large-field images. We used the methodology of Sheliga, Chen, Fitzgibbon, and Miles (Initial ocular following in humans: A response to first-order motion energy. *Vision Research*, 2005a), who studied the initial OFRs of humans, to study the initial OFRs of monkeys. Accordingly, we applied horizontal motion to: (1) vertical square-wave gratings lacking the fundamental (''missing fundamental stimulus'') and (2) vertical grating patterns consisting of the sum of two sinusoids of frequency 3*f* and 4*f*, which created a repeating pattern with beat frequency, *f*. Both visual stimuli share a critical property: when subject to 1/4-wavelength steps, their overall pattern (feature) shifts in the direction of the steps, whereas their major Fourier component shifts in the reverse direction (because of spatial aliasing). We found that the initial OFRs of monkeys to these stimuli, like those of humans, were always in the opposite direction to the 1/4-wavelength shifts, i.e., in the direction of the major Fourier component, consistent with detection by (low-level) oriented spatio-temporal filters as in the well-known energy model of motion analysis. Our data indicate that the motion detectors mediating the initial OFR have quantitatively similar properties in monkeys and humans, suggesting that monkeys provide a good animal model for the human OFR.


*Keywords:* Missing fundamental; Spatio-temporal filtering; Energy-based mechanisms; Eye movements

## 1. Introduction

In primates, sudden movements of the visual scene elicit ocular following responses (OFRs) with ultra-short latencies: <80 ms in humans and <60 ms in monkeys with some stimuli (Gellman, Carl, & Miles, 1990; Miles, Kawano, & Optican, 1986; Sheliga et al., 2005a, 2005b). It is believed that OFRs assist in the rapid stabilization of gaze with respect to the (stationary) surroundings (Miles, 1998), and there is substantial evidence that, in monkeys, it is mediated in large part by cortical area MST (Kawano, Inoue, Takemura, Kodaka, & Miles, 2000; Kawano, Shidara, Watanabe, & Yamane, 1994; Takemura, Inoue, & Kawano, 2002). Because the OFR is driven by retinal image motion, it has recently been used to study some of the neural processes underlying the sensing of visual motion in humans (Chen, Sheliga, Fitzgibbon, & Miles, 2005; Masson, Busettini, Yang, & Miles, 2001; Masson & Castet, 2002; Masson, Yang, &

* Corresponding author. Tel.: +81 75 753 4485; fax: +81 75 753 4486.
*E-mail address:* kmiura@brain.med.kyoto-u.ac.jp (K. Miura).

0042-6989/$ - see front matter © 2005 Elsevier Ltd. All rights reserved.
doi:10.1016/j.visres.2005.10.021

Miles, 2002; Sheliga et al., 2005a; Sheliga, Chen, Fitzgibbon, & Miles, 2005b; Yang & Miles, 2003). It is generally believed that there are at least two different neural mechanisms by which we analyze visual motion, and various descriptors have been applied to them, based in part on the methodology that was used to investigate them: see Lu and Sperling (2001) for review. One mechanism utilizes low-level visual motion detectors that are sensitive to luminance modulation, and functions without regard for form or features. This mechanism is variously referred to as, 1st-order, Fourier or energy-based. The other, high-level, mechanism(s) extracts visual motion using features to which the low-level visual motion detectors are insensitive, and is referred to as 2nd-order, non-Fourier or feature-based. We will use these various terms interchangeably, although they are not strictly synonymous.

Using special broad-band stimuli, Sheliga et al. (2005a, 2005b) recently demonstrated that the initial OFR in humans is largely determined by the motion of the principal Fourier component of the visual stimulus, as though reliant on oriented spatio-temporal visual filters as in the well-known energy model of motion detection, i.e., the human OFR is mediated by low-level motion detectors. These workers elicited OFRs with two kinds of apparent-motion stimuli whose features and principal Fourier components moved in opposite directions under the assumption that the brain gives the greatest weight to the nearest-neighbor matches (Georgeson & Harris, 1990; Hammett, Ledgeway, & Smith, 1993; see also Pantle & Turano, 1992). One was the missing fundamental (*mf*) stimulus, which can be constructed from a square wave by subtracting the fundamental sine-wave component. In the frequency domain, the *mf* stimulus consists of summed odd harmonics, the largest being the 3rd and the remainder having progressively decreasing amplitudes such that the *i*th harmonic has an amplitude proportional to $1/i$. Sheliga et al. (2005a, 2005b) moved the *mf* stimulus in discrete 1/4-wavelength steps rather than smoothly because, when so moved, all of its harmonics are shifted 1/4 of their wavelengths, the $4n+1$ harmonics (where $n$ is an integer) shifting in the direction of the actual image shifts (i.e., forwards, along with the entire pattern and its features), whereas the $4n-1$ harmonics (which include the principal Fourier component, the 3rd harmonic) shift in the opposite direction (i.e., backwards). Notice that a 3/4-wavelength forward shift of a pure sine-wave is exactly equivalent to a 1/4-wavelength backward shift because of spatial aliasing, and it is invariably the latter that determines the direction of any associated OFRs and perceived motion (Pantle & Turano, 1992). The other apparent-motion stimulus used by Sheliga et al. was the so-called 3*f*4*f* stimulus, which is a repeating pattern with a spatial-frequency of $f$ that is constructed by summing two sinusoids of equal-amplitude whose spatial frequencies are in the ratio 3:4, the 3*f* and 4*f* components (Hammett et al., 1993). When this pattern is shifted forwards in successive steps that are each 1/4 of the wavelength of the beat, the 4*f* component is effectively stationary while the 3*f* component steps backward 1/4 of its wavelength because of spatial aliasing, exactly as with the $4n-1$ harmonics of the *mf* stimulus. Sheliga et al. (2005a, 2005b) reported that the initial OFRs elicited by these *mf* and 3*f*4*f* stimuli in humans were invariably in the direction of motion of their principal Fourier component(s) rather than the direction of motion of their features, consistent with a mechanism that has oriented spatio-temporal filters and senses 1st-order motion (cf., Masson et al., 2002). Indeed, Sheliga et al. (2005a) have suggested that the initial OFR of humans provides a model system for studying neural sensors that respond selectively to 1st-order visual motion and do not respond to 2nd-order motion. Psychophysical studies indicate that when 1/4-wavelength steps are applied to *mf* stimuli human observers generally—but not always—perceive them to move in the opposite direction to their true motion (Adelson, 1982; Adelson & Bergen, 1985; Baro & Levinson, 1988; Brown & He, 2000; Georgeson & Harris, 1990; Georgeson & Shackleton, 1989). Also, human observers generally experience motion transparency when viewing 3*f*4*f* stimuli, seeing rapid forward motion of the beat and slower reverse motion of the 3*f* component, consistent with the simultaneous activation of feature-based (2nd-order) and energy-based (1st-order) sensing mechanisms, respectively (Hammett et al., 1993).

To further examine the neural mechanisms underlying the visual motion detectors underlying initial OFRs, it is critical to have an adequate animal model. We were interested in the monkey as one such model but were concerned by a previous report, based on one monkey, which concluded that the initial OFRs to motion defined by contrast modulated noise—a pure 2nd-order motion stimulus—were essentially the same as to motion defined by luminance modulations—1st-order motion—except for a very slight difference in latency (Benson & Guo, 1999). Further, there have been a number of reports that some neurons in the middle temporal area (MT) of the monkey are sensitive to 2nd-order motion (Albright, 1992; Ilg & Churan, 2004; O'Keefe & Movshon, 1998). We now report that the initial OFRs elicited in macaque monkeys when 1/4-wavelength steps are applied to *mf* and 3*f*4*f* stimuli are in all essentials like those described by Sheliga et al. (2005a) in humans—being dominated in large part by the 1st-order motion energy in the principal Fourier components—indicating that the monkey is a good animal model.

## 2. Methods

Data were collected from two rhesus monkeys (*Macaca fuscata*), weighing 7.7 (A) and 8.8 kg (B). All procedures reported here were approved by the Institute's Animal Care and Use Committee. Many of the general procedures were the same as those used in previous studies of ocular tracking in monkeys (Kawano et al., 1994; Kodaka, Miura, Suehiro, Takemura, & Kawano, 2004) and humans (Sheliga et al., 2005a) and so will only be given in brief.

### 2.1. Animal preparations

The monkeys were previously trained to fixate a small spot. Under pentobarbital sodium anesthesia and aseptic conditions, each monkey was implanted with a head holder, which allowed the head to be fixed in the standard stereotaxic position during the experiments, and a scleral search coil to allow measurement of the position of the right eye (Judge, Richmond, & Chu, 1980).

### 2.2. Visual display and stimuli

The animals faced a 19 in CRT monitor (Eizo T766, driven by a PC Radeon 9800 Pro video card), which was 50 cm in front of the eyes, in a dark room. Visual stimuli were presented on the monitor (resolution, 1280 × 1024 pixels; vertical refresh rate, 100 Hz). The RGB signals from the video card were converted to black and white images with 11-bit grayscale resolution through an attenuator (Pelli, 1997), exactly as described by Sheliga et al. (2005a). Briefly, a luminance look-up table with 256 equally spaced luminance levels ranging from 0.3 to 77.1 cd/m$^2$ was created by direct luminance measurements (LS-100 photometer; Konica-Minolta, Japan) under software control. This table was then expanded to 2048 equally spaced levels by interpolation.

The visual images consisted of one-dimensional vertical grating patterns that could have one of four horizontal luminance profiles in any given trial: (1) a square wave with a missing fundamental (*mf* stimulus), achieved by summing the odd harmonics (starting with the 3rd harmonic and finishing with the highest harmonic that fell short of the Nyquist frequency) as described by Sheliga et al. (2005a); (2) a sum of two equal-amplitude sinusoids whose spatial frequencies were in the ratio 3:4 (3*f*4*f* stimulus); (3) a pure sine-wave with the same frequency as the beat of the *mf* and 3*f*4*f* stimuli (1*f* stimulus); (4) a pure sine-wave whose spatial frequency was three times that of the 1*f* stimulus (3*f* stimulus), and hence was the same as that of the principal Fourier component of the *mf* stimulus (the 3rd harmonic) and the 3*f* component of the 3*f*4*f* stimulus. Each image extended 360 mm horizontally (39.6°; 1280 pixels) and 270 mm vertically (30.2°; 1024 pixels) and had a mean luminance of 38.7 cd/m$^2$. The initial phase of a given grating was randomized from trial to trial at intervals of 1/4-wavelength. Motion was created by substituting a new image every frame (i.e., every 10 ms) for a total of 15 frames (i.e., stimulus duration, 150 ms), each new image being identical to the previous one except phase shifted horizontally by 1/4 of the wavelength of the fundamental. In any given trial the successive steps were all in the same direction (rightward or leftward, randomly selected). We examined the OFRs elicited by these apparent-motion stimuli at various stimulus contrast levels (1, 2, 4, 8, 16, 32, and 64%, where the contrast was defined as, $((L_{max} - L_{min})/(L_{max} + L_{min}))*100\%$, $L_{max}$, and $L_{min}$ being the maximum and minimum luminance levels, respectively). An experimental block consisted of 56 stimulus entries (4 grating patterns, 2 directions of motion, and 7 contrast levels), all of which were interleaved and randomly ordered in individual blocks.

### 2.3. Procedures

At the beginning of each trial, a grating pattern appeared together with a central target spot (diameter, 0.4°) that the animal had been trained to fixate. After the monkey's right eye had been positioned within 2° of the fixation target for a randomized period of 750–1000 ms (and no saccades had been detected for the last 250 ms in this period), the fixation target disappeared and the apparent-motion stimulus began. Otherwise, the screen became uniform gray and the trial was repeated. The motion lasted for 150 ms, at which time the screen became a uniform gray with the same mean luminance. Then, the animals were rewarded with a drop of juice, signaling the end of the trial. After an inter-trial interval of 1000–1500 ms, a new grating pattern appeared together with a fixation point, commencing a new trial. Data were collected over several sessions until each condition had been repeated an adequate number of times to permit good resolution of the responses through averaging.

### 2.4. Data collection and analyses

All aspects of the experimental paradigms were controlled by two PCs, which communicated via Ethernet using the TCP/IP protocol. One of the PCs was running a Real-time EXperimentation software package (REX) developed by Hays, Richmond, and Optican (1982), and provided the overall control of the experimental protocol as well as acquiring, displaying, and storing the eye-movement data. The other PC was running Matlab subroutines, utilizing the Psychophysics Toolbox extensions (Brainard, 1997; Pelli, 1997), and generated the visual stimuli upon receiving a start signal from the REX machine.

Eye movements were measured using the electromagnetic search coil technique (Fuchs & Robinson, 1966). The voltage signals encoding the horizontal and vertical components of the eye position were passed through an analog low-pass filter (−3 dB at 200 Hz) and were digitized to a resolution of 12 bits, sampling at 1 kHz. All data were stored and transferred to another PC for analysis using computer programs based on Matlab (The Mathworks). The eye-position data were smoothed with a 3-pole digital butterworth filter (−3 dB at 30 Hz), and eye-velocity traces were derived from the two-point backward difference. Eye acceleration profiles were derived from the two-point backward difference of the eye-velocity traces, and were used to detect small saccades that went undetected during the experiment. Trials with saccadic intrusions were then discarded (on average, 23% in monkey A and 27% in monkey B). Mean temporal eye-velocity profiles were computed for each of the stimulus

conditions. To obtain low-noise estimates of eye-velocity, responses were averaged over at least 31 trials in the preliminary experiment on spatial-frequency and 40 trials in the main experiment on contrast.

The initial horizontal OFRs were quantified by measuring the changes in horizontal eye position over the 50-ms time periods starting 50 ms after the onset of the motion stimuli. The minimum latency of onset was ~50 ms so that these response measures were restricted to the period prior to the closure of the visual feedback loop (i.e., twice the reaction time): initial open-loop responses. The responses to rightward and leftward were pooled to improve the signal-to-noise ratio by subtracting the mean response to a given leftward motion stimulus from the mean response to the corresponding rightward motion stimulus, and these will be referred to the "R–L responses." The 95% confidence intervals were calculated to indicate the extent of the fluctuations in R–L measures. Because rightward eye movements were positive in our sign convention, these pooled R–L measures were positive when the OFR was in the direction of the applied image shift (also sometimes referred to as the "forward" direction, in contradistinction to the "backward" or "reverse" direction).

## 3. Results

### 3.1. Dependence on spatial-frequency

To determine what spatial-frequency to use for the *mf* and 3*f*4*f* stimuli, we did a preliminary experiment in which we applied 1/4-wavelength steps to pure sinusoidal vertical gratings (contrast, 32%) with a wide range of spatial frequencies (0.05, 0.10, 0.20, 0.40, 0.81, and 1.62 cycles/°). Fig. 1 shows the data obtained from both monkeys, with the mean R–L velocity traces over time above (A and C) and the associated mean R–L change-in-position measures plotted against spatial-frequency below (B and D). All OFRs were in the forward direction, which is positive in our convention (see Methods) and so they are rendered as upward deflections of the R–L velocity traces (from a zero baseline) in Figs. 1A and C. The R–L measures displayed clear band-pass dependence on spatial-frequency that was well-represented by Gaussian functions ($r^2$ values: 0.995, 0.996) with peaks ($f_o$) at 0.158, and 0.291 cycles/°

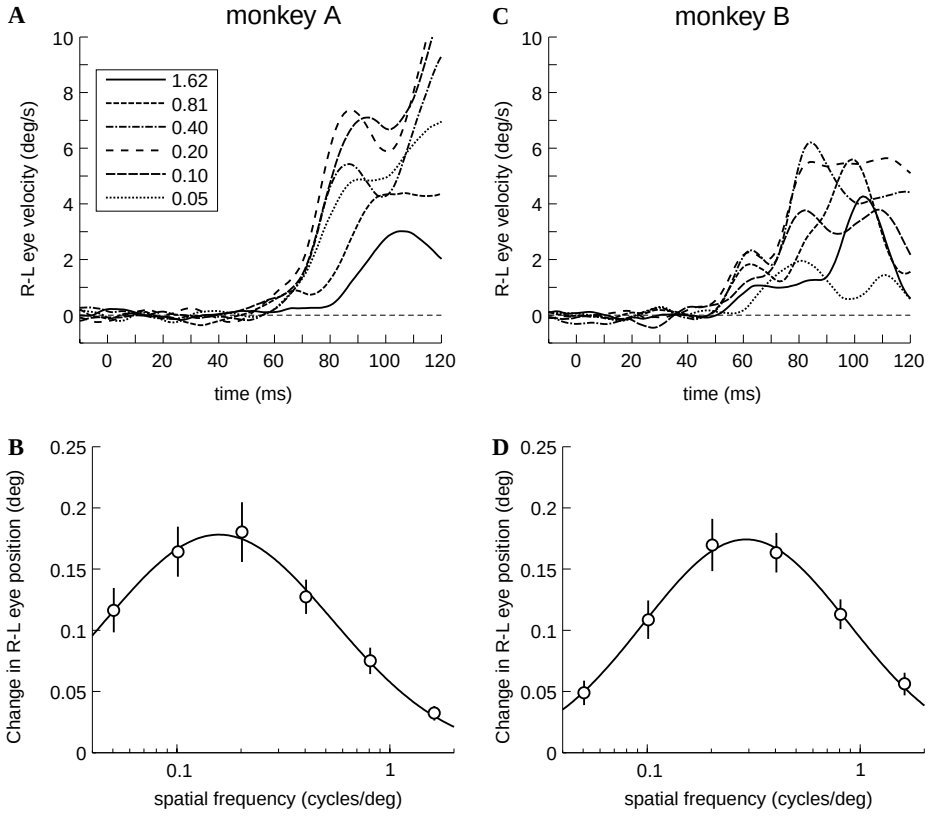


Fig. 1. The initial OFR elicited by 1/4-wavelength steps applied to sinusoidal grating patterns (1*f* stimulus): dependence on spatial-frequency (two monkeys). (A and C) Mean R–L eye-velocity temporal profiles: see key for spatial frequencies (in cycles/°). Upward deflections of the traces from the zero baseline (dashed horizontal line) denote forward motion (in the direction of the steps). Zero on the abscissa denotes the time of the first 1/4-wavelength shift (defined as the onset of stimulus motion). (B and D) Mean R–L response measures (mean change in R–L position during the time period 50–100 ms after the onset of motion) plotted as a function of the spatial-frequency in cycles/°; note that the abscissa has a logarithmic scale. The smooth curves are the best fit Gaussian functions: see Sheliga et al. (2005a) for methods. The data for monkey A are in (A and B) (31–37 trials per condition; SD's ranged 0.018–0.072°) and the data for monkey B are in (C and D) (59–73 trials per condition; SD's ranged 0.039–0.089°). Contrast, 32%. Error bars, 95% confidence intervals.

and standard deviations ($\sigma$) of 0.534 and 0.482 log units in monkey A and monkey B, respectively: see the continuous smooth curves in Figs. 1B and D and note the logarithmic abscissas. These parameters of the fitted Gaussian functions were used to derive a low-frequency cutoff ($f_{lo}$) and a high-frequency cutoff ($f_{hi}$), defined as the spatial frequencies at which the tuning curve was half its maximum, using the following expression from Read and Cumming (2003): $f_o \exp(\pm\sigma\sqrt{\ln 4})$. The computed values of $f_{lo}$ were 0.037, and 0.079 cycles/°, and the computed values of $f_{hi}$ were 0.672, and 1.077 cycles/°. The initial OFRs of humans show a very similar Gaussian dependence on log spatial-frequency (Sheliga et al., 2005a). Based on these findings, the fundamental spatial frequencies (*f*) selected for the *mf* and 3*f*4*f* stimuli were 0.09 cycles/° for monkey A and 0.15 cycles/° for monkey B, thereby ensuring that the initial OFRs elicited by pure sine-waves of spatial-frequency 1*f* and 3*f* were of similar amplitude.

### 3.2. Dependence on contrast

Fig. 2 shows the mean OFR temporal profiles (again, R–L responses) elicited from monkey A by successive discrete phase shifts applied to each of the four different grating patterns over a wide range of contrasts. The shifts always had the same absolute amplitude, 2.78°, which meant that with each shift the 1*f*, *mf*, and 3*f*4*f* gratings stepped forwards 1/4 of their wavelength (given that their wavelengths were all 11.1°), whereas the 3*f* grating stepped forwards 3/4 of its wavelength, which was equivalent to a *backward* step of 1/4 of its wavelength. Let us first consider the data obtained with the pure sine-wave stimuli. It is evident from Fig. 2 that the initial OFRs elicited by the 1*f* stimulus were always in the *forward* direction whereas those elicited by the 3*f* stimulus were always in the *backward* direction, exactly in accord with the shortest-path or nearest-neighbor matches for these stimuli: spatial aliasing. Of course, a pure sine-wave has only one Fourier component and this always shifts together with its features (peaks and troughs), so it is not possible to determine which of these two attributes of the motion stimulus elicited the OFR here. Turning to the more complex grating patterns, however, it is evident that the initial OFR elicited by the *mf* and 3*f*4*f* stimuli were always in the *backward* direction, which was the direction of motion of their

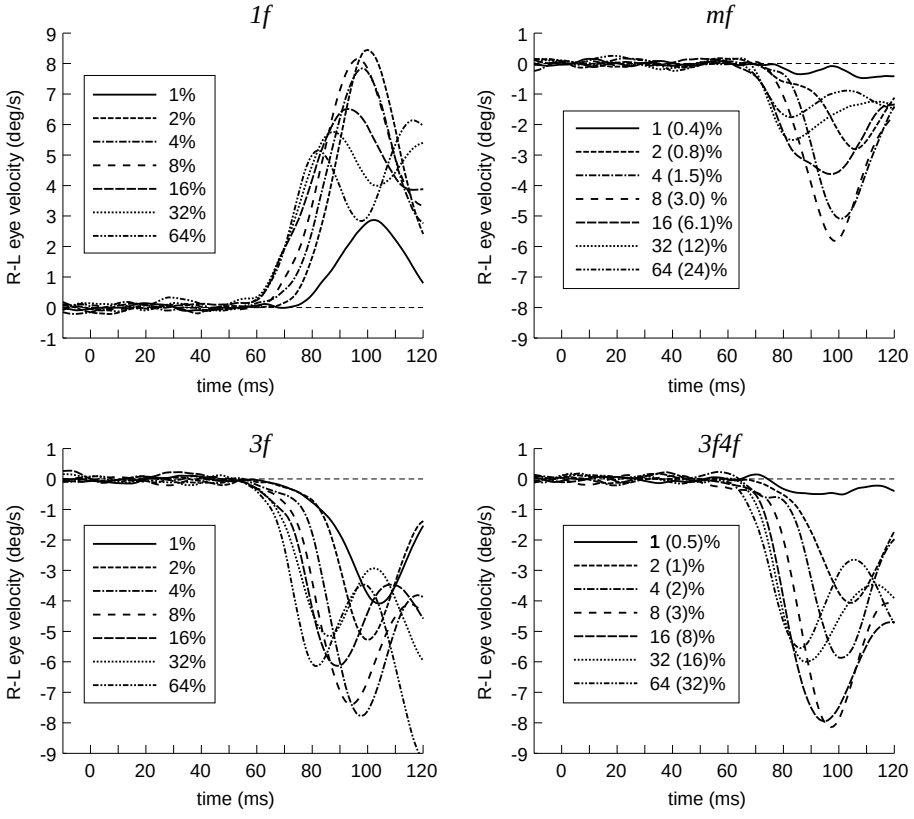


Fig. 2. The initial OFR: dependence on contrast (eye velocity traces from monkey A). All motion stimuli consisted of successive shifts that had the same absolute amplitude, 2.78°, which was 1/4 of the wavelength of the 1*f*, *mf*, and 3*f*4*f* gratings, whose fundamentals all had wavelengths of 11.1° (spatial frequencies, 0.09 cycles/°), and 3/4 of the wavelength of the 3*f* grating, whose wavelength was 3.7° (spatial-frequency, 0.27 cycles/°). Traces show the mean R–L eye-velocity temporal profiles. The keys indicate the contrasts, those values in parentheses for the *mf* and 3*f*4*f* data indicating the contrasts of the 3rd harmonic and 3*f* component, respectively. Upward deflections of the traces from the zero baselines (dashed horizontal lines) denote forward motion (in the direction of the steps). Abscissas denote the time from the first stimulus shift (defined as the onset of stimulus motion).

principal Fourier components (the 3rd harmonic and the 3*f* component, respectively) and opposite to the direction of motion of their features.

Let us scrutinize the response profiles in Fig. 2 more closely, starting with those obtained with the 1*f* stimulus (upper left). At the lowest contrast (1%), the initial transient OFR had a latency of 70–80 ms and reached a peak at ~100 ms after the onset of the apparent-motion (i.e., the time of the first step). As the stimulus contrast was increased to 2%, this initial transient showed a slight reduction in latency and a substantial increase in amplitude. Further increases in stimulus contrast resulted in shorter onset latencies with *reduced* initial peaks, which is the "anomalous contrast-dependence" originally described by Miles et al. (1986), who recorded the initial OFR elicited from monkeys when velocity steps were applied to pure sine-wave gratings. The response profiles obtained with the 3*f* stimulus (lower left in Fig. 2) show a similar general pattern even though of the opposite sign, as also do the profiles obtained with the *mf* stimulus (upper right in Fig. 2) and the 3*f*4*f* stimulus (lower right in Fig. 2), consistent with mediation largely by their 3*f* components. The profiles obtained with the *mf* stimulus, however, are clearly much lower in amplitude than those obtained with the other stimuli. The OFRs of the other monkey, which are not illustrated, showed the same general tendencies.

The anomalous reductions in the amplitude of the initial peak in the OFR profiles as contrast was increased beyond 2% were attributed by Miles et al. (1986) to a reduction in the time available to integrate the motion error signal because of the associated decreases in latency, and they successfully modeled this effect. Indeed, these workers also showed that no such anomalous dependence on contrast was apparent when the velocity responses were integrated over a fixed interval time-locked to motion onset and approximating the initial open-loop period, as though the reductions in velocity amplitude were offset by the reductions in the latency of response onset. We too found this same effect in our data and report it in Fig. 3, which shows the dependence on stimulus contrast of the initial OFR based on the changes in the mean R–L position measures over the time period 50–100 ms (measured from the time of the first step), for all four grating patterns and both monkeys. The R–L response measures for the data obtained with the 1*f* and 3*f* stimuli (filled and open circles in Fig. 3), generally showed a monotonic rise as the stimulus contrast increased, gradually saturating as contrast reached 5–10% in monkey A and 20–30% in monkey B (note the log abscissa). Of course, the 1*f* data all have positive values (being in the forward direction) and the 3*f* data all have negative values (being in the backward direction). These data were fitted with the following expression:

$$R_{\max}\frac{c^n}{c^n + c_{50}^n}, \tag{1}$$

where $R_{\max}$ is the maximum attainable response, $c$ is the contrast, $c_{50}$ is the semi-saturation contrast (at which the response has half its maximum value), and $n$ is the exponent that sets the steepness of the curves.

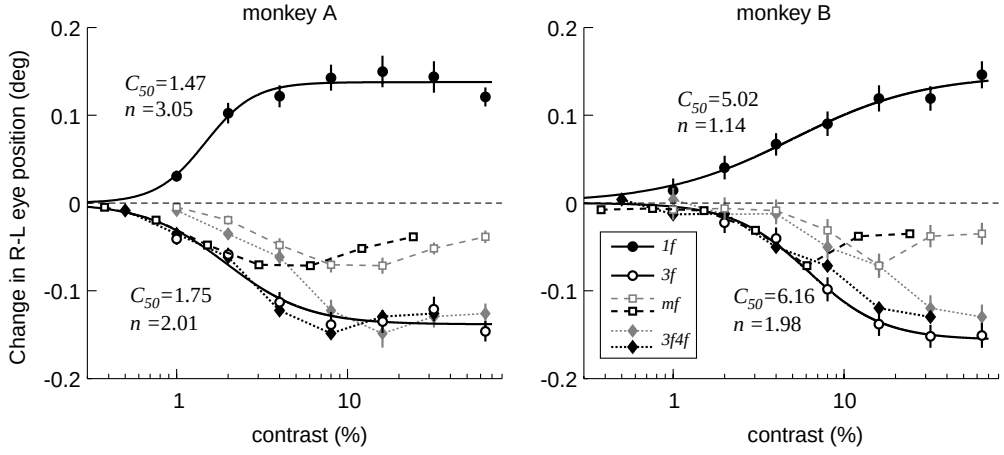


Fig. 3. The initial OFR: dependence on contrast (R–L response measures for two monkeys). Plots show the horizontal OFR elicited when successive steps (each 2.78° for monkey A and 1.67° for monkey B) were applied to *mf* and 3*f*4*f* stimuli (spatial frequencies and wavelengths: monkey A, 0.09 cycles/° and 11.1°; monkey B, 0.15 cycles/° and 6.67°) as well as to pure sine-wave gratings whose spatial frequencies matched the 1*f* or 3*f* components of the complex gratings. Responses to the pure 1*f* sine-waves (filled circles) were always positive (OFR in the forward direction), whereas those to the *mf* stimulus (gray open squares, gray dashed lines), the 3*f*4*f* stimulus (gray filled diamonds, gray dotted lines), and the pure 3*f* sine-waves (open circles) gratings were always negative (OFR in the backward direction). Responses to the *mf* and 3*f*4*f* gratings are also replotted as a function of the contrast of their 3*f* components to permit easy comparison with the pure 3*f* sine-wave data (*mf*, black open squares and dashed lines; 3*f*4*f*, black filled diamonds and dotted lines). The smooth black curves are best-fit Naka–Rushton functions for the pure sine-wave data and the values of their $c_{50}$ and $n$ parameters are shown nearby. Monkey A: 40–56 trials per condition; SD's ranged 0.017–0.062°. Monkey B: 40–54 trials per condition; SD's ranged 0.038–0.054°. Error bars, 95% confidence intervals.

This expression is based on the Naka–Rushton equation (Naka & Rushton, 1966) and provides a good fit to the contrast-dependence curves of neurons in the LGN, V1, and MT of monkeys (Albrecht, Geisler, Frazor, & Crane, 2002; Albrecht & Hamilton, 1982; Heuer & Britten, 2002; Sclar, Maunsell, & Lennie, 1990), as well as to the human contrast-dependence curves for the initial OFRs to moving sine-wave gratings (Sheliga et al., 2005a) and unikinetic plaid patterns (Masson & Castet, 2002). The continuous smooth curves in Fig. 3 are the best fit curves using this expression and are clearly good approximations to the data with $r^2$ values >0.9 for all curves. The values of $c_{50}$ for the 1*f* and 3*f* stimuli were 1.47 and 2.01%, respectively, for monkey A, and 5.02 and 6.16%, respectively, for monkey B. The values of $n$ for the 1*f* and 3*f* stimuli were 3.05 and 1.75, respectively, for monkey A, and 1.14 and 1.98, respectively, for monkey B. Thus, the OFRs were most sensitive to changes in contrast when the contrast was relatively low (<5% for monkey A and <20% for monkey B).

If the initial OFRs to the *mf* and 3*f*4*f* stimuli are actually generated by their principal Fourier components, the 3rd harmonic and the 3*f* component, respectively, then when plotted in terms of the contrast of these components, their contrast-dependence data should overlay those obtained with pure sine waves of the same spatial-frequency, i.e., the data obtained with the 3*f* stimulus. The data obtained with the *mf* stimulus (squares and dashed lines in Fig. 3) and the 3*f*4*f* stimulus (diamonds and dotted lines in Fig. 3) are therefore plotted as a function of both the actual contrast of the patterns (gray symbols and lines) and the contrast of their 3rd harmonic and 3*f* components (black symbols and lines). As we pointed out earlier, the OFRs to these *mf* and 3*f*4*f* stimuli were always in the opposite direction to the actual shifts of the patterns and so have negative values in Fig. 3. When plotted as a function of the contrast of their 3*f* component, the data obtained with the 3*f*4*f* stimulus approximated those obtained with the pure sine-wave 3*f* stimuli, though tending to fall a little short at higher contrasts in monkey B. When plotted as a function of the contrast of their 3rd harmonic, the data obtained with the *mf* stimulus also closely approximated those obtained with the 3*f* stimulus at low contrast (<3% for monkey A, <8% for monkey B), but fell substantially short of this with higher contrast stimuli. Very similar trends are seen in humans (Sheliga et al., 2005a).

For monkey A, the 3*f*4*f* data in Fig. 3 closely approximate the pure 3*f* data (when plotted as a function of the contrast of the 3*f* component), indicating that the 4*f* component of the 3*f*4*f* stimulus had almost no impact on the initial OFR measures, and this was also apparent from the R–L temporal response profiles: see Fig. 4 (left column) and compare the thick traces (the 3*f*4*f*-stimulus data) with the thin traces (the 3*f*-stimulus data). For monkey B, the 3*f*4*f*-stimulus data fell short of the 3*f*-stimulus data at high contrast and the R–L temporal profiles in Fig. 4 (right column) indicate that the impact of the 4*f* component was not uniform but rather selectively affected a small early transient component and a later sustained component (that was mostly outside the open-loop measurement period) and left the main body of the response profile largely intact.

## 4. Discussion

### 4.1. The monkey as a model for the human

Our data show that the initial OFRs of the monkey share many fundamental properties with those of the human recently described by Sheliga et al. (2005a, 2005b), indicating that the monkey provides an excellent animal model. The initial support for this conclusion comes from the data obtained with the pure sine-wave stimuli and these are further reinforced by the data obtained with the more complex *mf* and 3*f*4*f* stimuli. Let us start by comparing the quantitative R–L response measures obtained with pure sine-wave stimuli in the two studies. The initial OFRs of our monkeys and of Sheliga et al.'s humans showed a dependence on spatial-frequency that was clearly band-pass and well described by Gaussian functions (with a log abscissa). Even the parameters of the best-fit Gaussians were very similar in the two species. For example, mean values for the three humans in the Sheliga et al. study vs. mean values for our two monkeys were as follows: $f_o = 0.25$ vs 0.22 cycles/°; $\sigma = 0.51$ vs 0.51 log units; $f_{lo} = 0.06$ vs 0.06 cycles/°; $f_{hi} = 0.99$ vs 0.87 cycles/°. The dependence on contrast also had a very similar form in monkeys and humans, showing a smooth monotonic rise with saturation at moderate contrast levels that was well-fit by the Naka–Rushton equation, whose parameters were again quite similar in our two studies (even though the data from the two monkeys showed much more scatter than the data from the three humans). For example, the mean best-fit Naka–Rushton parameters for the 1*f* data (human vs monkey) were as follows: $c_{50} = 3.9$ vs 3.24%; $n = 2.10$ vs 2.09, and the equivalent 3*f* data are: $c_{50}$=5.7 vs 4.09%; $n = 1.55$ vs 1.87. Nonetheless, the anomalous dependency on contrast that is evident in the initial peak of the monkey's eye-velocity traces in both our study and that of Miles et al. (1986), whereby over part of the contrast range, *increases* in contrast were associated with *decreases* in the amplitude of the initial peak in eye-velocity, is not seen in the temporal profiles of the human OFR (Sheliga et al., 2005a). This anomaly presumably had no obvious impact on our integrated-velocity measures that were time-locked

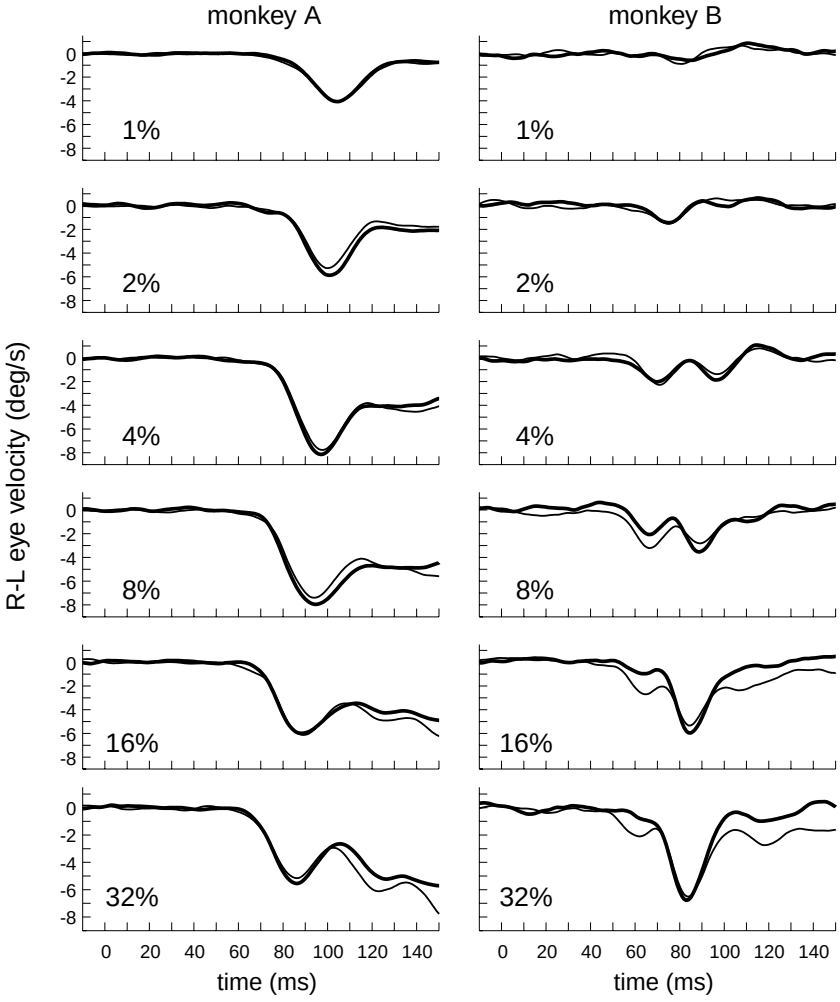


Fig. 4. Comparison of the OFRs elicited by 3*f* and 3*f*4*f* stimuli with a range of contrasts (temporal profiles for two monkeys). All shifts and wavelengths were as given in the legend of Fig. 3. Each panel shows the mean R–L temporal velocity profiles elicited by the 3*f* stimulus alone (thin line), and the 3*f*4*f* stimulus (thick line) whose 3*f* component had a contrast that matched that of the 3*f* stimulus and is listed on each plot (in %). All responses deflected the traces downward from the zero baseline, denoting backward eye movements (in the direction of the principal Fourier component). Abscissas denote the time from the first stimulus shift (defined as the onset of stimulus motion).

to stimulus onset (i.e., the change-in-position measures in Fig. 3) because of the associated latency changes, as originally pointed out by Miles et al. (1986). In fact, the latency of the monkey's OFR (to smoothly drifted sinusoidal gratings) is solely a function of contrast and temporal frequency (Miles et al., 1986), whereas the latency of the human's OFR is also somewhat sensitive to speed and spatial-frequency (Gellman et al., 1990) and less sensitive to contrast (see Fig. 5 of Sheliga et al., 2005a). However, these detailed differences in the latency and development of the very earliest OFRs of monkeys and humans ultimately have little consequence for the overall tracking responses as indicated by the similarity of their integrated-velocity measures over the initial open-loop period.

Our study showed that the initial OFRs elicited by the *mf* and 3*f*4*f* stimuli were *always* in the direction of their principal Fourier components (i.e., the 3*f* component of the 3*f*4*f* stimulus and the 3rd harmonic of the *mf* stimulus) rather than in the direction of the overall pattern or feature. In fact, the 4*f* component of the 3*f*4*f* stimulus often had almost no impact on the monkey's initial OFR, including the temporal profiles (Fig. 4). Thus, when the R–L response measures obtained with the 3*f*4*f* stimuli were plotted in terms of the contrast of their 3*f* component, they matched the measures obtained with the pure 3*f* stimulus quite closely (except in monkey B at higher contrasts, when they fell slightly short). Similar plots of the data obtained with the *mf* stimulus—using the contrast of the 3rd harmonic rather than of the whole pattern—mimicked the plots for the 3*f* stimuli only at low contrasts and then fell progressively short with higher contrast. These data are all very similar to those obtained on humans by Sheliga et al. (2005a), further reinforcing the view that the monkey is a good animal model for the initial OFR of humans.

### 4.2. The initial OFR: A response to 1st-order motion energy

Sheliga et al. (2005a) argued that the dependence on the motion of the principal Fourier components of the *mf* and 3*f*4*f* stimuli—rather than on the motion of their features—indicated that the motion detectors responsible for the initial OFR in humans do not operate directly on the raw retinal images but rather on a spatially filtered version of those images, as in the well-known 1st-order energy model of motion detection that relies on oriented spatio-temporal filters: see Lu and Sperling (2001) for review. Using *mf* stimuli lacking the 5th and 7th harmonics, Sheliga et al. (2005a) were also able to show that the initial OFRs elicited by the usual *mf* stimulus fell short of those elicited by the pure 3*f* stimulus mostly because of the higher harmonics, with perhaps a very minor contribution from distortion products due to an early compressive non-linearity in the visual pathway. Thus, Sheliga et al. largely ruled out even a minor rôle for feature-based mechanisms in the genesis of the initial OFR of humans. Although we do not have data for the monkey that clarifies the role of the higher harmonics, we have demonstrated that the monkey's initial OFR shares much in common with that of the human. Further, the similarity of the contrast-dependence of the 3*f*4*f* and pure 3*f* data is consistent with mediation by oriented spatio-temporal filters as in the 1st-order motion-energy model and indicates that feature-based mechanisms make at best only a minor contribution to the monkey's OFR with this 3*f*4*f* stimulus.

Sensitivity to low-contrast stimuli (<20%), such as we here report for the monkey's OFR, is considered one of the characteristics that, in humans, sets the 1st-order motion energy mechanisms apart from feature-based mechanisms (Lu & Sperling, 1995; Nishida, 1993; Smith, 1994; Solomon & Sperling, 1994; Takeuchi & De Valois, 1997). Consistent with this, the study of O'Keefe and Movshon (1998) on monkeys showed that MT neurons have poor contrast-sensitivity for 2nd-order motion. Yet, Benson and Guo (1999) reported that the initial OFRs to a pure 2nd-order motion stimulus (defined by contrast modulated noise) were little different from those to a stimulus with strong 1st-order motion energy (except for a small latency difference, averaging ~11 ms). This observation, which was made only on a single monkey, would seem to be at odds with our findings, perhaps suggesting that some types of 2nd-order motion are much more effective in initiating OFR than others.

## 5. Closing remarks

Earlier studies in monkeys (Busettini, Miles, & Schwarz, 1991; Kawano & Miles, 1986; Miles et al., 1986) and humans (Busettini, Miles, Schwarz, & Carl, 1994; Gellman et al., 1990) demonstrated a number of functional similarities between the OFRs of the two species which fostered the idea that the monkey was a good animal model for the human. Our present findings on the initial OFRs elicited in monkeys by motion applied to complex grating patterns are largely in accord with the findings in a recent study on humans that used these same visual stimuli (Sheliga et al., 2005a), suggesting that the similarities between the two species extend to the detectors whereby they sense visual motion.

## Acknowledgments

This work was supported by the JSPS.KAKENHI (#16GS0312), the MEXT.KAKENHI (#17700309), the Japan-US Brain Research Cooperative Program, and the Intramural Research Program of the NIH, the National Eye Institute.

## References

Adelson, E. H. (1982). Some new motion illusions, and some old ones, analysed in terms of their Fourier components. *Investigative Ophthalmology & Visual Science, 34*(Suppl.), 144, Abstract.

Adelson, E. H., & Bergen, J. R. (1985). Spatiotemporal energy models for the perception of motion. *Journal of the Optical Society of America A, 2*, 284–299.

Albrecht, D. G., Geisler, W. S., Frazor, R. A., & Crane, A. M. (2002). Visual cortex neurons of monkeys and cats: Temporal dynamics of the contrast response function. *Journal of Neurophysiology, 88*, 888–913.

Albrecht, D. G., & Hamilton, D. B. (1982). Striate cortex of monkey and cat: Contrast response function. *Journal of Neurophysiology, 48*, 217–237.

Albright, T. D. (1992). Form-cue invariant motion processing in primate visual cortex. *Science, 255*, 1141–1143.

Baro, J. A., & Levinson, E. (1988). Apparent motion can be perceived between patterns with dissimilar spatial frequencies. *Vision Research, 28*, 1311–1313.

Benson, P. J., & Guo, K. (1999). Stages in motion processing revealed by the ocular following response. *Neuroreport, 10*, 3803–3807.

Brainard, D. H. (1997). The psychophysics toolbox. *Spatial Vision, 10*, 433–436.

Brown, R. O., & He, S. (2000). Visual motion of missing-fundamental patterns: motion energy versus feature correspondence. *Vision Research, 40*, 2135–2147.

Busettini, C., Miles, F. A., & Schwarz, U. (1991). Ocular responses to translation and their dependence on viewing distance. II. Motion of the scene. *Journal of Neurophysiology, 66*, 865–878.

Busettini, C., Miles, F. A., Schwarz, U., & Carl, J. R. (1994). Human ocular responses to translation of the observer and of the scene: Dependence on viewing distance. *Experimental Brain Research, 100*, 484–494.

Chen, K. J., Sheliga, B. M., Fitzgibbon, E. J., & Miles, F. A. (2005). Initial ocular following in humans depends critically on the Fourier components of the motion stimulus. *Annals of the New York Academy of Sciences, 1039*, 260–271.

Fuchs, A. F., & Robinson, D. A. (1966). A method for measuring horizontal and vertical eye movement chronically in the monkey. *Journal of Applied Physiology, 21*, 1068–1070.

Gellman, R. S., Carl, J. R., & Miles, F. A. (1990). Short latency ocular-following responses in man. *Visual Neuroscience, 5*, 107–122.

Georgeson, M. A., & Harris, M. G. (1990). The temporal range of motion sensing and motion perception. *Vision Research, 30*, 615–619.

Georgeson, M. A., & Shackleton, T. M. (1989). Monocular motion sensing, binocular motion perception. *Vision Research, 29*, 1511–1523.

Hammett, S. T., Ledgeway, T., & Smith, A. T. (1993). Transparent motion from feature- and luminance-based processes. *Vision Research, 33*, 1119–1122.

Hays, A. V., Richmond, B. J., & Optican, L. M. (1982). A UNIX-based multiple process system for real-time data acquisition and control. *WESCON Conference Proceedings, 2*, 1–10.

Heuer, H. W., & Britten, K. H. (2002). Contrast dependence of response normalization in area MT of the rhesus macaque. *Journal of Neurophysiology, 88*, 3398–3408.

Ilg, U. J., & Churan, J. (2004). Motion perception without explicit activity in areas MT and MST. *Journal of Neurophysiology, 92*, 1512–1523.

Judge, S. J., Richmond, B. J., & Chu, F. C. (1980). Implantation of magnetic search coils for measurement of eye position: An improved method. *Vision Research, 20*, 535–538.

Kawano, K., Inoue, Y., Takemura, A., Kodaka, Y., & Miles, F. A. (2000). The role of MST neurons during ocular tracking in 3D space. *International Review of Neurobiology, 44*, 49–63.

Kawano, K., & Miles, F. A. (1986). Short-latency ocular following responses of monkey. II. Dependence on a prior saccadic eye movement. *Journal of Neurophysiology, 56*, 1355–1380.

Kawano, K., Shidara, M., Watanabe, Y., & Yamane, S. (1994). Neural activity in cortical area MST of alert monkey during ocular following responses. *Journal of Neurophysiology, 71*, 2305–2324.

Kodaka, Y., Miura, K., Suehiro, K., Takemura, A., & Kawano, K. (2004). Ocular tracking of moving targets: Effects of perturbing the background. *Journal of Neurophysiology, 91*, 2474–2483.

Lu, Z. L., & Sperling, G. (1995). The functional architecture of human visual motion perception. *Vision Research, 35*, 2697–2722.

Lu, Z. L., & Sperling, G. (2001). Three-systems theory of human visual motion perception: Review and update. *Journal of the Optical Society of America A, 18*, 2331–2370.

Masson, G. S., Busettini, C., Yang, D.-S., & Miles, F. A. (2001). Short-latency ocular following in humans: Sensitivity to binocular disparity. *Vision Research, 41*, 3371–3387.

Masson, G. S., & Castet, E. (2002). Parallel motion processing for the initiation of short-latency ocular following in humans. *The Journal of Neuroscience, 22*, 5149–5163.

Masson, G. S., Yang, D. S., & Miles, F. A. (2002). Reversed short-latency ocular following. *Vision Research, 42*, 2081–2087.

Miles, F. A. (1998). The neural processing of 3-D visual information: Evidence from eye movements. *The European Journal of Neuroscience, 10*, 811–822.

Miles, F. A., Kawano, K., & Optican, L. M. (1986). Short-latency ocular following responses of monkey. I. Dependence on temporospatial properties of visual input. *Journal of Neurophysiology, 56*, 1321–1354.

Naka, K. I., & Rushton, W. A. (1966). S-potentials from colour units in the retina of fish (Cyprinidae). *Journal of Physiology, 185*, 536–555.

Nishida, S. (1993). Spatiotemporal properties of motion perception for random-check contrast modulations. *Vision Research, 33*, 633–645.

O'Keefe, L. P., & Movshon, J. A. (1998). Processing of first- and second-order motion signals by neurons in area MT of the macaque monkey. *Visual Neuroscience, 15*, 305–317.

Pantle, A., & Turano, K. (1992). Visual resolution of motion ambiguity with periodic luminance- and contrast-domain stimuli. *Vision Research, 32*, 2093–2106.

Pelli, D. G. (1997). The VideoToolbox software for visual psychophysics: Transforming numbers into movies. *Spatial Vision, 10*, 437–442.

Read, J. C., & Cumming, B. G. (2003). Testing quantitative models of binocular disparity selectivity in primary visual cortex. *Journal of Neurophysiology, 90*, 2795–2817.

Sclar, G., Maunsell, J. H., & Lennie, P. (1990). Coding of image contrast in central visual pathways of the macaque monkey. *Vision Research, 30*, 1–10.

Sheliga, B. M., Chen, K. J., Fitzgibbon, E. J., & Miles, F. A. (2005a). Initial ocular following in humans: A response to first-order motion energy. *Vision Research, 45*, 3307–3321.

Sheliga, B. M., Chen, K. J., Fitzgibbon, E. J., & Miles, F. A. (2005b). Short-latency disparity vergence in humans: Evidence for early spatial filtering. *Annals of the New York Academy of Sciences, 1039*, 252–259.

Smith, A. T. (1994). Correspondence-based and energy-based detection of second-order motion in human vision. *Journal of the Optical Society of America A, 11*, 1940–1948.

Solomon, J. A., & Sperling, G. (1994). Full-wave and half-wave rectification in second-order motion perception. *Vision Research, 34*, 2239–2257.

Takemura, A., Inoue, Y., & Kawano, K. (2002). Visually driven eye movements elicited at ultra-short latency are severely impaired by MST lesions. *Annals of the New York Academy of Sciences, 956*, 456–459.

Takeuchi, T., & De Valois, K. K. (1997). Motion-reversal reveals two motion mechanisms functioning in scotopic vision. *Vision Research, 37*, 745–755.

Yang, D. S., & Miles, F. A. (2003). Short-latency ocular following in humans is dependent on absolute (rather than relative) binocular disparity. *Vision Research, 43*, 1387–1396.